

## Ankaramites of Gorny Altai: Mineralogical, Petrographic, and Petrochemical Features of Diopside Porphyry Basalts of the Ust'-Sema Formation

N. Khlif<sup>a,c</sup>, A.V. Vishnevskiy<sup>a,b,✉</sup>, A.E. Izokh<sup>a,b</sup>

<sup>a</sup> Novosibirsk State University, ul. Pirogova 1, Novosibirsk, 630090, Russia

<sup>b</sup> V.S. Sobolev Institute of Geology and Mineralogy, Siberian Branch of the Russian Academy of Sciences, pr. Akademika Koptuyuga 3, Novosibirsk, 630090, Russia

<sup>c</sup> Al-Furat University, Deir ez-Zur, Syria

Received 28 December 2018; received in revised form 5 June 2019; accepted 28 August 2019

**Abstract**—The mineral composition, petrography, and petrochemistry of middle Cambrian diopside porphyry basalts of the Ust'-Sema Formation in Gorny Altai are considered in comparison with ankaramites of different geodynamic settings. The basalts of the Ust'-Sema Formation are enriched in phenocrysts of high-Mg clinopyroxene ( $Mg\# \leq 94$ ) (20 to 40–50 vol.%) with a high content of  $Cr_2O_3$  (up to 1.11 wt.%), enclosed in the clinopyroxene–plagioclase microlitic groundmass. In addition, there are minor phenocrysts of saussuritized plagioclase ( $An_{49-71}$ ), olivine replaced by secondary minerals, amphibole with  $Mg\# = 55.7-68.2$ , and Cr-spinel with  $Cr\# = 36.2-41.7$ . Inclusions of Cr-spinel in high-Mg clinopyroxene are richer in Cr ( $Cr\# \leq 72.8$ ). The basalts of the Ust'-Sema Formation are chemically heterogeneous and are subdivided into two main groups: high-Ca ( $MgO = 7.98-14.77$  wt.% and  $CaO/Al_2O_3 = 1.0-1.8$ ) and low-Ca ( $MgO = 2.84-9.89$  wt.% and  $CaO/Al_2O_3 = 0.2-0.9$ ). The obtained data on the high-Ca basalts of the Ust'-Sema Formation show that the rocks are similar to the reviewed ankaramites and thus can be assigned to this type of rocks. The low-Ca basalts of the Ust'-Sema Formation might have resulted from the fractionation of ankaramitic melt in intermediate magma chambers. The Gorny Altai ankaramites formed through the melting of the wehrlitized suprasubduction lithospheric mantle during the closure of the Paleasian Ocean.

**Keywords:** Ankaramite, high-Ca magma, clinopyroxene, Cr-diopside, Ural–Alaskan type, island arc magmatism, accretionary magmatism, middle Cambrian, Gorny Altai

### INTRODUCTION

The nature of mafic magmatism during the Neoproterozoic–early Paleozoic stage of evolution of the Altai–Sayan folded area, in particular, of middle Cambrian diopside porphyry basalts of the Ust'-Sema Formation in Gorny Altai (Buslov et al., 1993, 2001; Gibsher et al., 1997; Dobretsov et al., 2004; Zybin, 2006; Simonov et al., 2010; Safonova et al., 2011), is a controversial issue. These rocks are significantly enriched in clinopyroxene phenocrysts (up to 40–50 vol.%). Some researchers assign these basalts to boninites, because they have high contents of  $SiO_2$ , Mg, Ni, and Cr (Dobretsov et al., 2004). According to the criteria of the IUGS (International Union of Geological Sciences) classification of igneous rocks, these rocks cannot be considered boninites but should be referred to as basalts enriched in diopside phenocrysts, i.e., diopside porphyry basalts (Gibsher et al., 1997). In conformance with the modern international classification of igneous rocks, volcanics with

pyroxene dominating over olivine are either ankaramites or boninites (Le Maitre et al., 2002). Boninites (both high- and low-Ca ones) contain orthopyroxene (enstatite or bronzite) or clinoenstatite, and ankaramites contain clinopyroxene (diopside) (Della-Pasqua and Varne, 1997; Le Maitre et al., 2002).

The existence and genesis of ankaramitic (high-Ca) magma have been actively discussed for a long time (Barsdell and Berry, 1990; Della-Pasqua and Varne, 1997; Schiano et al., 2000; Kogiso and Hirschmann, 2001; Green et al., 2004; Portnyagin et al., 2005a,b; Médard et al., 2006; Elburg et al., 2007; Marchev et al., 2009; Sorbadere et al., 2013). This type of magma is observed both as lavas (volcanic rocks) enriched in clinopyroxene phenocrysts and as high-Ca melt inclusions in olivine or clinopyroxene phenocrysts from ankaramites or basalts (Schiano et al., 2000). The great interest in the problem of identification and classification of ankaramites is due to the fact that some researchers assume that ankaramites are the parental magma for platinum-bearing gabbro–pyroxenite–dunite intrusions of the Ural–Alaskan type (Irvine, 1973; Pushkarev et al., 2018). Pushkarev and Gottman (2016) studied the volcanics of the Irendyk

✉ Corresponding author.

E-mail address: vishnevsky@igm.nsc.ru (A.V. Vishnevskiy)

Formation being part of the Gadel'sha and Karsaklyktau volcanic edifices in the melange of the West Magnitogorsk zone near Abzakovo Village in the South Urals. They discovered and studied clinopyroxene porphyrites with an extremely high content of phenocrysts, up to 25–35% and higher. These rocks compose bombs in volcanic breccias. They are also found as subvolcanic bodies, stocks, and dikes. The same forms of occurrences are specific to diopside porphyry basalts of the Ust'-Sema Formation. The composition evolution of clinopyroxenes and Cr-spinels in the Irendyk porphyrites is identical both to the evolution trend of ankaramite and to the primary magmatic evolution trend of Cr-spinel in dunite–clinopyroxenite complexes of the Ural–Alaskan type. This supports the viewpoint that ankaramites are parental magma for platinum-bearing intrusions (Pushkarev and Gottman, 2016). In addition, Cr-spinel phenocrysts from the Urals ankaramites contain isoferroplatinum inclusions, which proves that these rocks are comagmatic with the Urals platinum-bearing intrusions (Gottman et al., 2016). In the Altai–Sayan folded area (Kuznetsk Alatau, Gornaya Shoria, and Salair), gold placers with ferroplatinum were found (Izokh et al., 2004; Zhmodik et al., 2016). The composition of their platinum-group minerals makes it clear that the platinum-bearing province formed as a result of the erosion of bodies genetically similar in composition to intrusions of the Ural–Alaskan type, but the primary sources of Pt has not been established yet (Tolstykh, 2004). In western Mongolia, ferroplatinum placers are confined to the early Cambrian Ureg Nuur volcanoplutonic picrite–basalt association, which includes diopside porphyry basalts similar to the rocks of the Ust'-Sema Formation (Oyunchimeg et al., 2009; Izokh et al., 2010).

The goal of this research was to demonstrate that part of the diopside porphyry basalts of the Ust'-Sema Formation should be classified as ankaramites. For this purpose it was necessary to establish the specific features of ankaramites and compare them with the data on the objects under study, namely, the well-preserved and comprehensively studied Biika and Ust'-Sema volcanic edifices (Buslov et al., 1993; Gibsher et al., 1997; Zybin, 2006; Simonov et al., 2010; Safonova et al., 2011).

### THE GEOLOGIC AND GEODYNAMIC SETTINGS OF DIOPSIDE PORPHYRY BASALTS OF THE UST'-SEMA FORMATION

The Ust'-Sema Formation is part of the Katun' accretionary complex (northern Gorny Altai), which is, in turn, part of the accretionary prism of the Kuznetsk–Altai island arc formed on the margin of the Siberian continent as a result of the late Neoproterozoic–Cambrian subduction of the Paleasian oceanic crust (Buslov et al., 2001; Dobretsov et al., 2004).

The basalts of the Ust'-Sema Formation are localized primarily in two central-type volcanic edifices, Ust'-Sema and

Biika, in the northwest and southeast of the Katun' zone, respectively (Fig. 1). The Biika Volcano crops out along the Katun' River in the interfluvium of the Choburak, Biika, Tymkesken, and Karasu Rivers and is almost isometric in shape (6.0×8.5 km) (Fig. 1b). Basalts also compose the Anos–Emurla linear structure more than 90 km in length between the two volcanic centers (Zybin, 2006) (Fig. 1). The Ust'-Sema Formation also includes flows of pyroxene porphyry and pyroxene–plagioclase porphyry basalts, their differentiates, agglomerates, pyroclastic breccias, and tuffs. Basalts in different volcanic edifices of the Ust'-Sema Formation and in the remote outcrops have a similar petrographic composition (Zybin, 2006).

The rocks of the Ust'-Sema Formation rest upon the Neoproterozoic–lower Cambrian Cheposh and Manzherok Formations (Fig. 1) and are overlain, with an angular unconformity, by the Elanda Formation containing trilobites typical of the upper part of the middle Cambrian (Zybin, 2006; Fedak et al., 2011). The rocks are associated with dikes and the Apshiyakhta, Elanda, and Barangol ultramafic–mafic subvolcanic bodies of the Barangol complex (Gibsher et al., 1997). There are different concepts of reconstruction of the geodynamic setting of the volcanics formation. Taking into account the geologic position of the rocks and their association with Neoproterozoic–early Cambrian basalts, some researchers reconstruct a back-arc paleobasin setting (Gibsher et al., 1997). Others, having analyzed the available geochemical and geological data, assume an intricate rock formation process during the subduction of the oceanic lithosphere into the subduction zone and subsequent melting of the rocks in the suprasubductional setting at the crust–upper-mantle boundary (Simonov et al., 2010; Safonova et al., 2011). We have studied the diopside porphyry basalts of the Biika volcanic edifice of the Ust'-Sema Formation with regard to the earlier analytical data (Buslov et al., 1993; Gibsher et al., 1997; Simonov et al., 2010; Safonova et al., 2011).

### METHODS

Samples were taken within the Biika volcanic edifice of the Ust'-Sema Formation in the area of the Biika River (fourteen samples of the early volcanic rocks) and in outcrops located southeast of this structure (two samples) (Fig. 1). Thin and polished sections were prepared from the samples for petrographic study. Some sampled clinopyroxene phenocrysts were mounted in epoxy-resin blocks. The blocks and the polished sections were examined using an Oxford X-Max 80 energy-dispersive spectrometer with a Tescan Mira 3 scanning electron microscope (SEM) at the Analytical Center for Multi-Elemental and Isotope Research SB RAS of V.S. Sobolev Institute of Geology and Mineralogy, Novosibirsk. Operation conditions: spectrum acquisition time, 20–30 s; voltage, 20 kV; and current, 10 nA. The error in measurement was 0.4–3.0% for major

components and 4–7% for trace elements. The detection limit of the components was 0.01–0.02% ( $3\sigma$  criterion) (Lavrent'ev et al., 2015). The spectral data were processed using the INCA Energy software. The bulk composition of

the rocks was analyzed by X-ray fluorescence analysis (XRF) on a Thermo Scientific ARL–9900 XP spectrometer at the Analytical Center for Multi-Elemental and Isotope Research SB RAS.

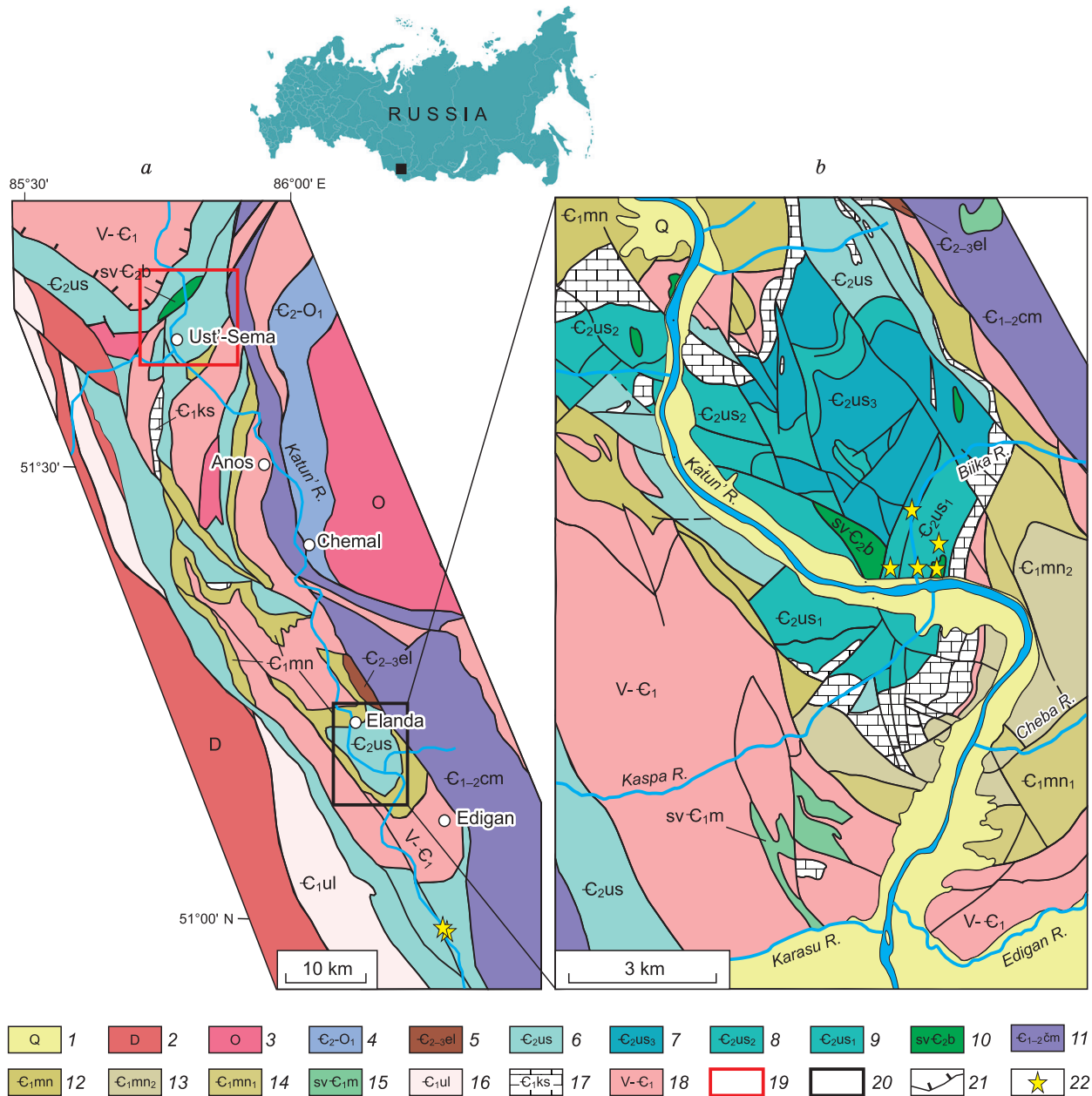


**Fig. 1.** Schematic geological map of northern Gorny Altai (a), after Fedak et al. (2011), simplified, and schematic geological map of the Biika volcanic edifice of the Ust'-Sema Formation in Gorny Altai (b), after Zybin (2006), simplified. 1, Quaternary sediments; 2, Devonian sediments; 3, Ordovician sediments; 4, thick flyschoid stratum of the Gorny Altai Group; 5, siltstones, sandstones, and shales of the Elanda Formation; 6–9, Ust'-Sema Formation: 6, undivided, 7, upper part (late stage of volcanism): pyroxene and plagioclase–pyroxene basalts and clastic lava rocks, 8, middle part (second phase): orthotuffites, tuffites, tuffs, and tuff breccias, 9, lower part (first phase): pyroxene and pyroxene–plagioclase basalts; 10, Barangol complex (linear gabbro, pyroxenite, and diorite bodies and stocks); 11, siltstones and siliceous-argillaceous shales of the Chermal Formation; 12–14, Manzhelok Formation: 12, undivided, 13, upper part: red-colored aphyric and fine-porphyrific plagioclase basalts, 14, lower part: green–dark-colored aphyric and fine-porphyrific basalts; 15, lower Cambrian subvolcanic bodies; 16, siliceous–carbonate–volcanic facies of the Uluscherga Formation; 17, Kaspia Group uniting the Cheposh and Shashkunar Formations, siltstones, siliceous-argillaceous shales, and argillaceous limestones; 18, Neoproterozoic–early Cambrian deposits; 19, 20, volcanic edifices of the Ust'-Sema Formation: 19, Ust'-Sema, 20, Biika (study area); 21, thrusts; 22, sampling localities.

## THE PETROGRAPHIC AND MINERAL COMPOSITIONS OF THE DIOPSIDE PORPHYRY BASALTS OF THE UST'-SEMA FORMATION

The basalts of the Biika volcanic edifice of the Ust'-Sema Formation are gray to dark gray, with a green tint, a massive structure, and a porphyritic texture (Fig. 2a, b). The groundmass is usually of microlitic texture (Fig. 2e). The rocks contain phenocrysts of clinopyroxene and altered plagioclase (Fig. 2a, b, e). Sometimes, completely altered phenocrysts of olivine and scarce grains of Cr-spinel and amphibole are present (Fig. 2c, d, f). The content of clinopyroxene phenocrysts reaches 50 vol.% in the pyroxene porphyry basalts and is lower in the pyroxene–plagioclase porphyry basalts (Fig. 2a, b).

**Clinopyroxene** phenocrysts are elongate prismatic and 0.5–25 mm (most often, 2–5 mm) in size. Their content is within 15–25 vol.%, sometimes reaching 40–50 vol.% (Figs. 2a, b and 3a, d). Most phenocrysts are clearly zoned both in transmitted light and in BSE images (Figs. 2a, b and 3a, d). The cores are composed mainly of diopside  $\text{En}_{42-49}\text{Wo}_{44-48}\text{Fs}_{4-11}$  with  $\text{Mg}\# = 92.4-81.7$  ( $\text{Mg}\# = 100 \cdot \text{Mg}/(\text{Mg} + \text{Fe})$ ), a high content of  $\text{Cr}_2\text{O}_3$  (up to 1.11 wt.%), and low contents (wt. %) of  $\text{TiO}_2$  (0.13–0.62),  $\text{Al}_2\text{O}_3$  (0.79–

3.97), and  $\text{Na}_2\text{O}$  (up to 0.27) (Figs. 3c, f and 4; Table 1). The rims consist of diopside and augite  $\text{En}_{34-45}\text{Wo}_{39-51}\text{Fs}_{9-21}$  ( $\text{Mg}\# = 83.3-66.0$ ); the latter has higher contents (wt.%) of  $\text{TiO}_2$  (0.32–1.82),  $\text{Al}_2\text{O}_3$  (2.53–8.99), and  $\text{Na}_2\text{O}$  (up to 0.61) and a lower content of  $\text{Cr}_2\text{O}_3$  (<0.5 wt.%) (Figs. 3c, f and 4; Table 1). Some phenocrysts show a reverse zoning, with  $\text{Mg}\# = 72.8$  in the core and 82.2 in the rim. The small crystals and the rims of the large ones show an oscillatory zoning, with  $\text{Mg}\# = 69-81$  in the cores and 66–82 on the periphery. Compared with the clinopyroxenes from the Ust'-Sema volcanic edifice (Buslov et al., 1993; Gibsher et al., 1997; Simonov et al., 2010), the earliest clinopyroxenes from the Biika volcanic edifice have a high  $\text{Mg}\#$  value (up to 94), a high content of  $\text{Cr}_2\text{O}_3$  (up to 1.1 wt.%), and very low contents of  $\text{TiO}_2$  ( $\leq 0.5$  wt.%) and  $\text{Al}_2\text{O}_3$  ( $\leq 3$  wt.%) (Fig. 4a–c).

In general, clinopyroxene from the basalts of the Ust'-Sema Formation is characterized by a negative correlation of  $\text{Mg}\#$  with the  $\text{TiO}_2$  and  $\text{Al}_2\text{O}_3$  contents and its positive correlation with the  $\text{Cr}_2\text{O}_3$  content (Fig. 4a–c; Table 1). The  $\text{Al}_2\text{O}_3$  content drastically increases from 2–3 wt.% in the cores to 7–9 wt.% in the rims and then decreases to 3–5 wt.% and <2 wt.% in the groundmass microlites (Fig. 4b). This indicates the existence of the stage of melt enrichment with

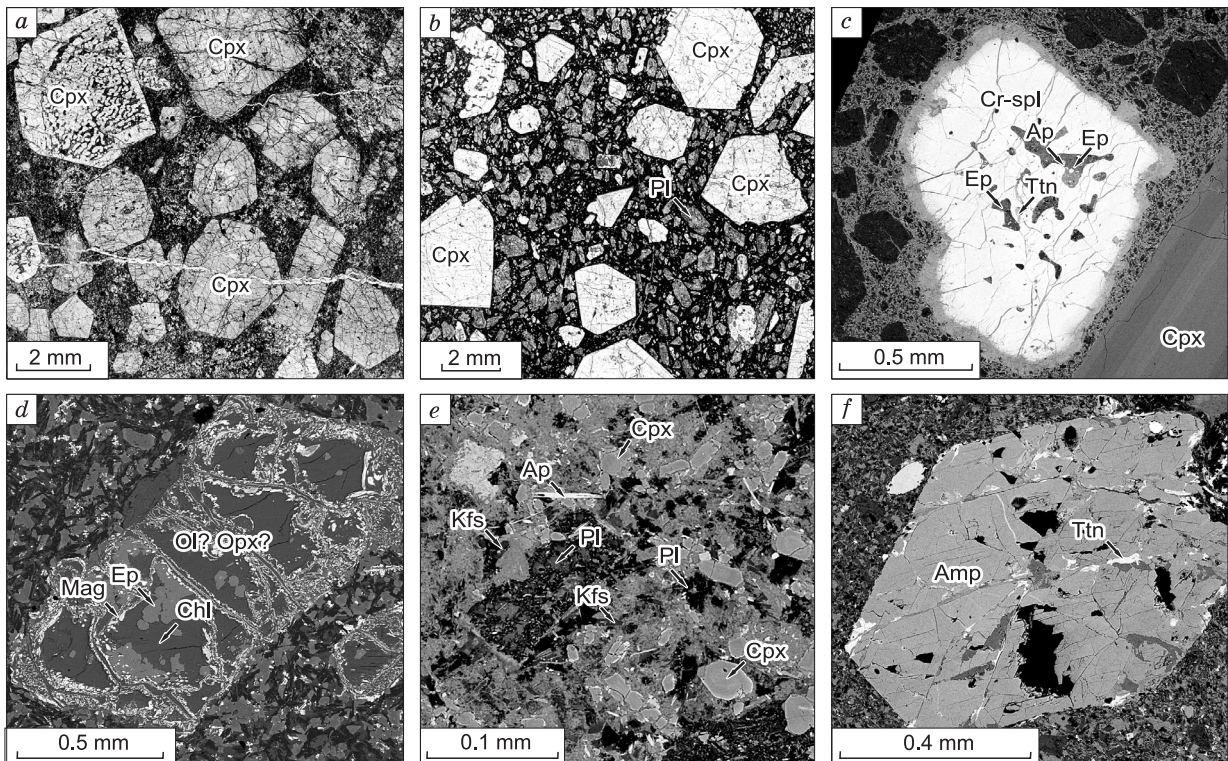


**Fig. 2.** Photomicrographs of diopside porphyry basalts of the Biika volcanic edifice (Ust'-Sema Formation). a, b, Transmitted-light images of thin sections: a, clinopyroxene phenocrysts in pyroxene porphyry basalts, b, fine phenocrysts of altered plagioclase and clinopyroxene phenocrysts in pyroxene–plagioclase porphyry basalts; c–f, BSE images of rock-forming minerals: c, single Cr-spinel phenocryst with epidote, apatite, and titanite inclusions, d, epidote–chlorite pseudomorphs developed after olivine phenocrysts, e, fine phenocryst of altered plagioclase and composition of groundmass, f, phenocryst of amphibole with titanite inclusion. Minerals: Cpx, clinopyroxene, Cr-spl, Cr-spinel, Ap, apatite, Ep, epidote, Ttn, titanite, Ol, olivine, Opx, orthopyroxene, Chl, chlorite, Kfs, K-feldspar, Pl, plagioclase, Amp, amphibole, Mag, magnetite.

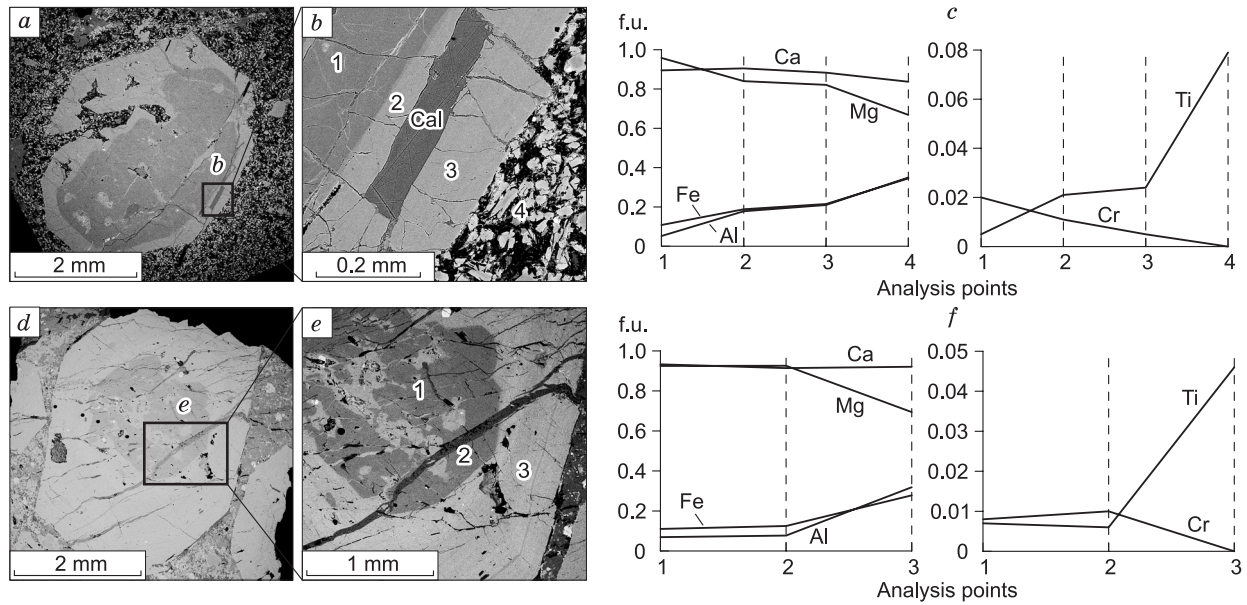


**Fig. 3.** Compositional variations of clinopyroxene phenocrysts from diopside porphyry basalts of the Biika volcanic edifice (Ust'-Sema Formation). *a, d*, BSE images of clinopyroxene phenocrysts (general view); *b, e*, BSE images of magnified fragments of their rims, with analysis points; *c, f*, contents of elements (Ca, Mg, Al, Fe, Ti, and Cr) per six oxygen atoms. Cal, calcite.

Al and the subsequent addition of plagioclase to the olivine–clinopyroxene cotectic curve. Some samples, however, do not show a significant increase in the alumina content (Fig. 4*b*).

**Plagioclase** occurs as fine ( $\leq 1$  mm) phenocrysts in pyroxene–plagioclase porphyry basalts, amounting to 50 vol.% (Fig. 2*b*). In pyroxene porphyry basalts, plagioclase is present mostly as microlites in the groundmass. The phenocrysts

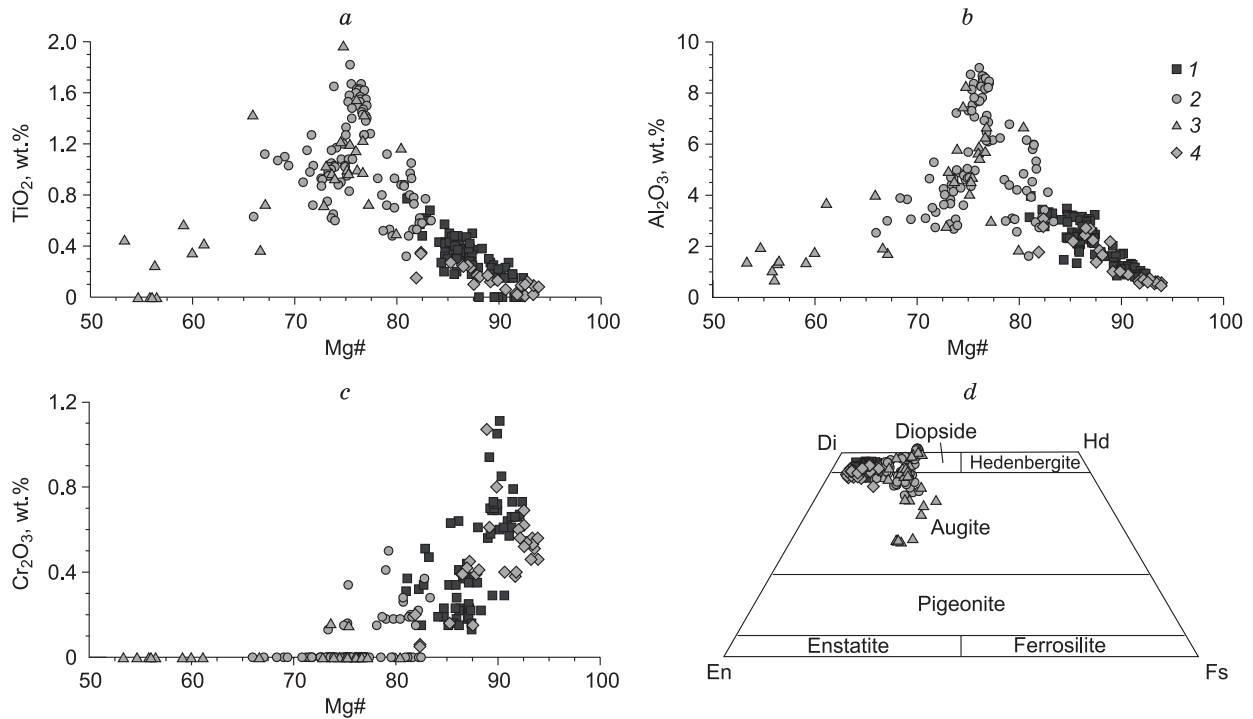


**Fig. 4.** Composition of clinopyroxenes from diopside porphyry basalts of the Ust'-Sema Formation.

*a–c*, Compositional variations of clinopyroxene; *d*, classification of pyroxenes (Morimoto, 1988). 1–3, clinopyroxenes from the Biika volcanic edifice (our data): 1, phenocryst core, 2, phenocryst rim, 3, clinopyroxene in the groundmass; 4, clinopyroxenes from the Ust'-Sema volcanic edifice (Buslov et al., 1993; Gibsher et al., 1997; Simonov et al., 2010).

**Table 1.** Representative analyses (wt.%) of clinopyroxene phenocrysts and microlites from diopside porphyry basalts of the Biika volcanic edifice of the Ust'-Sema Formation

Run	SiO <sub>2</sub>	TiO <sub>2</sub>	Al <sub>2</sub> O <sub>3</sub>	Cr <sub>2</sub> O <sub>3</sub>	FeO*	MgO	CaO	Na <sub>2</sub> O	Total	Mg#
1	53.61	N.f.	0.85	0.73	3.43	17.93	22.92	0.20	99.68	90.3
2	52.33	0.38	3.00	0.44	4.49	16.38	23.32	N.f.	100.35	87.0
3	53.36	0.23	1.21	0.29	3.16	17.30	23.84	N.f.	99.39	90.6
4	53.06	0.17	1.68	1.05	3.38	17.26	23.49	0.19	100.28	89.9
5	53.68	N.f.	0.87	0.79	2.83	17.96	23.58	N.f.	99.70	91.5
6	52.59	0.30	1.87	0.23	4.88	16.58	23.06	0.23	99.96	85.8
7	53.36	0.25	1.61	0.29	3.59	16.96	23.81	H.O.	99.87	89.5
8	52.63	0.23	1.78	0.35	4.04	16.82	23.10	0.12	99.07	88.0
9	54.06	0.18	1.21	0.70	3.58	17.74	23.06	0.20	100.74	89.2
10	49.03	0.73	5.03	N.f.	6.57	14.49	22.86	0.24	99.15	81.7
11	46.25	1.62	7.12	N.f.	8.75	12.24	22.60	0.44	99.02	76.8
12	50.77	0.77	4.12	0.37	6.12	15.34	23.00	0.23	100.87	82.8
13	51.15	0.52	2.99	0.19	7.59	15.07	21.83	0.30	99.77	78.7
14	49.21	1.03	3.34	N.f.	10.72	13.17	21.31	N.f.	99.20	71.8
15	45.63	1.63	8.67	N.f.	9.22	11.21	23.27	0.49	100.13	76.4
16	50.25	0.88	4.84	0.18	7.00	14.97	22.40	0.22	100.93	80.4
17	48.67	1.05	4.53	N.f.	9.67	13.48	21.07	0.40	99.21	73.6
18	55.90	N.f.	0.70	N.f.	13.25	16.28	13.18	0.18	99.74	56.0
19	52.35	0.50	1.87	N.f.	7.19	14.64	22.33	0.36	99.25	79.9
20	46.12	1.22	7.48	N.f.	10.09	11.18	23.00	0.39	99.74	74.5
21	47.60	1.23	6.29	N.f.	8.95	12.04	22.95	0.44	99.51	76.7
22	49.01	1.20	4.72	0.15	8.85	13.71	21.21	0.34	99.42	75.4
23	48.78	0.97	4.55	0.16	9.60	13.63	20.93	0.34	99.20	73.6

Note. 1–10, clinopyroxene from the phenocryst core; 11–17, clinopyroxene from the phenocryst rim; 18–23, microlites from the groundmass. Here and in Tables 2–4, N.f., not found, the analyses were carried out with an Oxford X-Max 80 energy-dispersive spectrometer with a Tescan Mira 3 scanning electron microscope at the Institute of Geology and Mineralogy, Novosibirsk.

\*Total iron as FeO.

are tabular and slightly elongated as compared with the groundmass microlites (Fig. 2e). Most of the plagioclase is saussuritized. In the preserved relics it is represented by bytownite and labradorite An<sub>49–71</sub> (Fig. 2e, Table 2). In the groundmass, plagioclase also corresponds to bytownite–labradorite An<sub>50–71</sub> (Table 2).

**Amphibole** is found as rare prismatic phenocrysts (0.1–0.7 mm). One of the studied samples contains 5–10 vol.% amphibole (Fig. 2f). The phenocrysts are unzoned (Fig. 2f) and correspond to magnesiohastingsite and, more seldom, pargasite (Table 3). Amphibole has Mg# = 55.7–68.2 and TiO<sub>2</sub> = 2.32–3.97 wt.% (Table 3).

**Cr-spinel** was found as a single phenocryst <1 mm in size (Fig. 2c). The mineral occurs mostly as fine inclusions in clinopyroxene (Mg# = 90). The composition of Cr-spinel phenocryst and inclusions is given in Table 4. The phenocryst has low contents of Cr<sub>2</sub>O<sub>3</sub> (<27 wt.%) and MgO (<3.75 wt.%), high contents of Al<sub>2</sub>O<sub>3</sub> (8.11–12.47 wt.%) and TiO<sub>2</sub> (4.67–5.35 wt.%), Cr# = 36.2–41.7, Mg# < 17, and Fe# = 30.7–43.6 (Table 4). The inclusions are characterized by Cr# = 69.7–72.8, Mg# = 51.4–55.4, Fe# < 13, and TiO<sub>2</sub> < 1 wt.% (Table 4).

**Olivine** is present as rare (<5 vol.%; usually, 1–2 vol.%) phenocrysts no larger than 1 mm (Fig. 2d). It is completely altered by an aggregate of chlorite, epidote, and magnetite (Fig. 2d).

**The groundmass** consists of clinopyroxene (augite and diopside (En<sub>31–49</sub>Wo<sub>28–50</sub>Fs<sub>7–26</sub>)) and plagioclase (An<sub>50–71</sub>) microlites (Fig. 2e). There are also xenomorphic grains of K–Na-feldspar (Ab<sub>2.5–99.3</sub>Or<sub>0.8–95.7</sub>), apatite, quartz, muscovite, magnetite, and calcite (Fig. 2e).

#### THE PETROCHEMICAL COMPOSITION OF THE DIOPSIDE PORPHYRY BASALTS OF THE UST'-SEMA FORMATION

To study the petrochemical composition of the Ust'-Sema Formation basalts, we used earlier representative analytical data on the rocks composing the Biika and Ust'-Sema volcanic edifices (Gibsher et al., 1997; Safonova et al., 2011) (partly listed in Table 5) and our data on the Biika rocks. The basalts are characterized by a wide variation in SiO<sub>2</sub> contents (44.58–56.40 wt.%). In the TAS classification

**Table 2.** Representative analyses (wt.%) of plagioclase phenocrysts and microlites from diopside porphyry basalts of the Biika volcanic edifice of the Ust'-Sema Formation

Analysis	SiO <sub>2</sub>	Al <sub>2</sub> O <sub>3</sub>	FeO*	MgO	CaO	Na <sub>2</sub> O	K <sub>2</sub> O	Total	An
1	54.87	28.88	0.58	N.f.	9.73	4.84	1.11	100.01	49.1
2	50.30	25.87	2.28	0.28	17.25	3.61	0.41	100.00	71.1
3	51.45	29.63	1.33	N.f.	13.39	3.63	0.36	99.78	65.7
4	54.20	28.90	0.58	N.f.	9.88	4.81	0.90	99.27	50.3
5	48.87	31.43	1.51	0.42	14.42	2.85	0.49	99.99	71.5

Note. 1, 2, phenocrysts; 3–5, microlites from the groundmass.

**Table 3.** Representative analyses (wt.%) of amphibole phenocrysts from diopside porphyry basalts of the Biika volcanic edifice of the Ust'-Sema Formation

Analysis	SiO <sub>2</sub>	TiO <sub>2</sub>	Al <sub>2</sub> O <sub>3</sub>	FeO*	MgO	CaO	Na <sub>2</sub> O	K <sub>2</sub> O	Total	Mg#
1	42.53	2.50	11.87	15.31	12.55	11.05	2.20	0.60	98.61	59.4
2	42.64	3.02	12.05	14.41	12.19	11.01	2.18	0.83	98.83	60.1
3	40.18	3.97	12.30	15.66	11.06	11.50	2.26	1.00	98.38	55.7
4	41.01	2.84	12.43	13.64	12.75	11.43	2.31	0.61	97.40	62.5
5	41.03	2.70	12.19	13.89	12.74	11.25	2.25	0.65	97.03	62.0
6	41.16	2.52	11.47	13.33	12.84	11.29	2.25	0.72	95.97	63.2
7	41.59	2.49	11.68	16.26	11.76	11.03	2.14	0.73	98.09	56.3
8	41.57	2.84	12.00	15.67	11.96	11.31	2.31	0.73	98.59	57.6
9	40.67	2.90	13.43	11.45	13.48	11.82	2.09	0.75	96.79	67.7
10	40.13	2.55	14.15	11.78	13.90	12.16	2.13	0.87	97.68	67.8
11	40.13	2.49	14.38	11.76	13.83	12.23	2.10	0.90	97.82	67.7
12	39.24	2.40	14.62	11.55	13.60	12.05	2.09	0.95	96.50	67.7
13	40.65	2.32	13.53	12.25	13.18	12.19	2.01	0.94	97.06	65.7
14	40.31	2.52	14.32	11.91	13.61	12.24	2.05	0.83	97.80	67.1
15	39.79	2.44	14.19	11.63	13.98	12.37	2.12	0.88	97.39	68.2

Note. 1–3, pargasites; 4–15, magnesiohastingsites; Mg# = 100·Mg/(Mg + Fe).

**Table 4.** Representative analyses (wt.%) of Cr-spinel phenocryst and inclusions from diopside porphyry basalts of the Biika volcanic edifice of the Ust'-Sema Formation

Analysis	SiO <sub>2</sub>	TiO <sub>2</sub>	Al <sub>2</sub> O <sub>3</sub>	Cr <sub>2</sub> O <sub>3</sub>	FeO*	Fe <sub>2</sub> O <sub>3</sub> *	V <sub>2</sub> O <sub>3</sub>	MnO	MgO	Total	Mg#	Cr#	Fe#
1	N.f.	4.67	12.47	26.63	21.06	32.02	N.f.	0.85	3.57	99.16	16.6	40.8	30.7
2	N.f.	4.87	10.35	26.10	22.06	35.59	0.37	1.90	0.45	100.30	2.2	41.7	33.6
3	0.41	5.35	8.11	21.62	27.42	36.25	0.57	1.90	0.39	100.35	1.9	36.2	43.6
4	N.f.	0.87	8.12	54.78	8.84	17.81	0.16	0.48	10.58	100.75	51.4	72.8	11.2
5	N.f.	0.88	8.31	52.62	10.14	16.18	N.f.	0.56	11.29	99.51	55.4	70.5	12.9
6	N.f.	0.97	8.77	52.27	10.19	16.66	N.f.	0.36	11.33	99.68	54.8	69.7	12.9

Note. 1–3, phenocryst; 4–6, inclusions in clinopyroxenes; Mg# = 100·(Mg/(Mg + Fe<sup>2+</sup>)); Cr# = 100·Cr/(Cr + Al); Fe# = 100·Fe<sup>3+</sup>/(Fe<sup>3+</sup> + Al + Cr).

\*The contents of FeO and Fe<sub>2</sub>O<sub>3</sub> were calculated from the total iron content, based on the stoichiometric compositions.

diagram, their composition points are in the fields of basalts, basaltic andesites, trachybasalts, and, more seldom, picobasalts and basaltic trachyandesites (Fig. 5a). The other major components also show wide variations in contents (wt.%): MgO = 2.84–11.58 (in one sample, 14.77), TiO<sub>2</sub> = 0.27–1.24 (in one sample, 1.52), CaO = 3.47–14.48, Al<sub>2</sub>O<sub>3</sub> = 7.51–21.29, Fe<sub>2</sub>O<sub>3</sub> = 6.72–13.52, K<sub>2</sub>O = 0.09–4.43,

and Na<sub>2</sub>O = 0.15–4.20 (Fig. 5b–f, Table 5). For this reason, the diopside porphyry basalts of the Ust'-Sema Formation were divided into several petrochemical groups: high-Mg, low-alumina, aluminous, Ti-containing, low-Mg, and K-containing (Gibsher et al., 1997; Safonova et al., 2011). However, the above authors did not take into account the high content of Ca and, accordingly, the high CaO/Al<sub>2</sub>O<sub>3</sub>

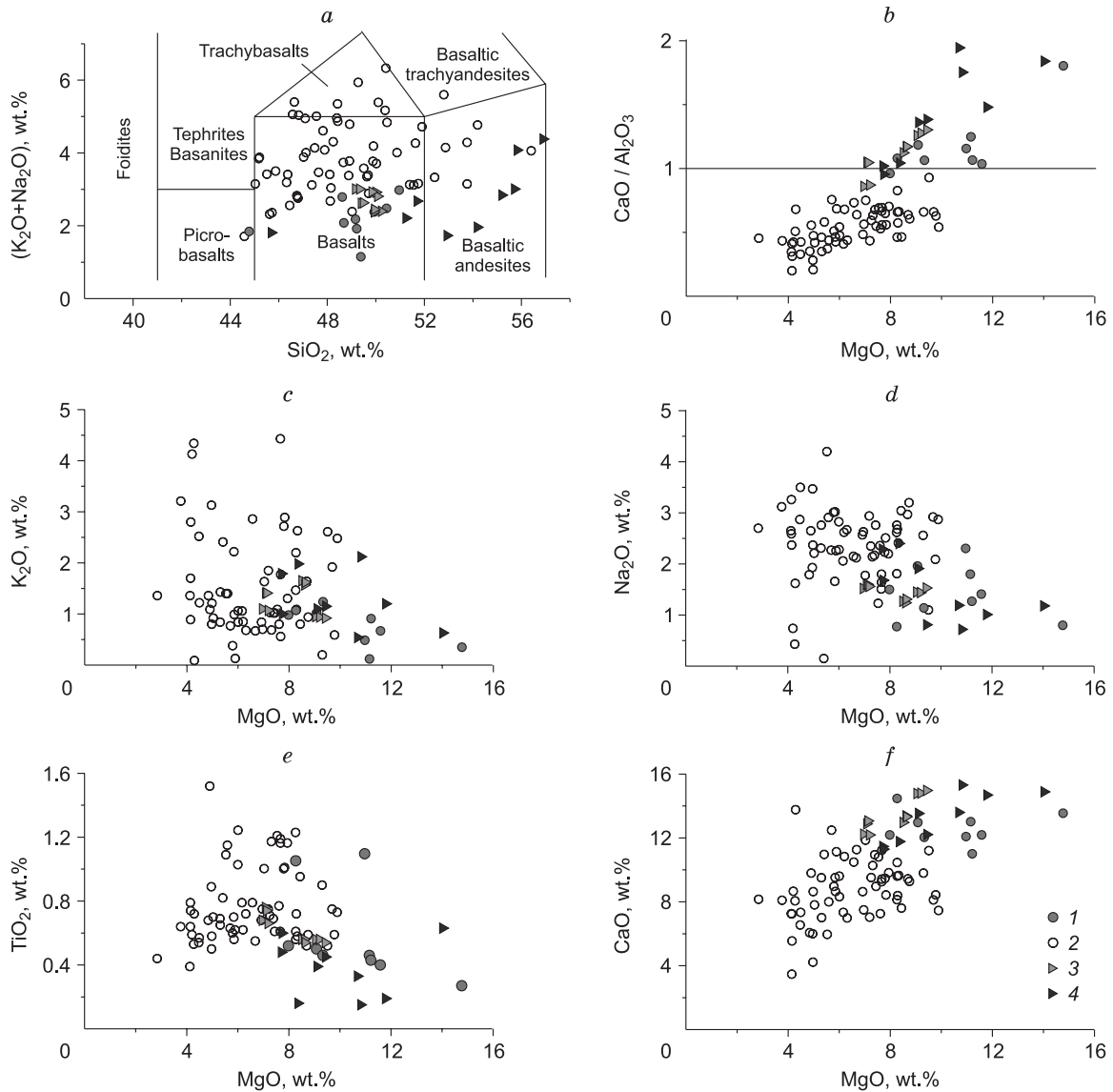


**Fig. 5.** Classification diagrams and chemical variations of diopside porphyry basalts of the Ust'-Sema Formation.

1, 2, Diopside porphyry basalts: 1, high-Ca group (ankaramites), 2, low-Ca group; 3, 4, homogenized melt inclusions in clinopyroxenes from the basalts: 3, (Simonov et al., 2010), 4, (Buslov et al., 1993).

ratios typical of volcanics enriched in clinopyroxene phenocrysts, i.e., ankaramites (Fig. 5b, Table 5).

Based on this criterion, we have recognized two groups of the basalts, high-Ca and low-Ca, although the ranges of their absolute CaO contents significantly overlap (Fig. 5f, Table 5). The low-Ca rocks have high contents (wt.%) of SiO<sub>2</sub> (44.58–56.40), Al<sub>2</sub>O<sub>3</sub> (12.07–21.29), Fe<sub>2</sub>O<sub>3</sub> (6.72–13.52), TiO<sub>2</sub> (0.39–1.52), K<sub>2</sub>O (0.09–4.43), and Na<sub>2</sub>O (0.15–4.20), low contents of MgO (2.84–9.89) and CaO (3.47–13.77), and low CaO/Al<sub>2</sub>O<sub>3</sub> ratios (0.2–0.9) (Fig. 5, Table 5). The high-Ca basalts have high contents (wt.%) of MgO (7.98–14.77) and CaO (11.01–14.48), high CaO/Al<sub>2</sub>O<sub>3</sub> ratios (1.0–1.8), and low contents of SiO<sub>2</sub> (44.78–50.96), Al<sub>2</sub>O<sub>3</sub> (7.51–13.41), TiO<sub>2</sub> (0.27–1.10), Fe<sub>2</sub>O<sub>3</sub> (9.27–11.18), K<sub>2</sub>O (0.12–1.24), and Na<sub>2</sub>O (0.77–2.30) (Fig. 5, Table 5).

In addition to the analysis of the bulk composition of the basalts, we studied their petrochemical features using data on the composition of homogenized melt inclusions found in high-Mg (Mg# > 82) clinopyroxene from the Ust'-Sema Volcano basalts from two sites: on the right bank of the Katur' River between Ust'-Sema and Cheposh Villages (Buslov et al., 1993) and in the eastern part of the Cherga area, 16 km southwest of Ust'-Sema Village (Simonov et al., 2010). The composition points of these inclusions are in the fields of basalts and basaltic andesites (Fig. 5a). The homogenized melt inclusions in clinopyroxene from the Cherga basalts have a narrow range of the contents of all rock-forming components (SiO<sub>2</sub> = 49.22–50.29, TiO<sub>2</sub> = 0.54–0.76, Na<sub>2</sub>O = 1.24–1.60, MgO = 7.01–9.48 wt.%, and CaO/Al<sub>2</sub>O<sub>3</sub> = 0.9–1.3) as compared with the melt inclusions in

**Table 5.** Representative analyses (wt.%) of the Ust'-Sema Formation basalts

Sample	SiO <sub>2</sub>	TiO <sub>2</sub>	Al <sub>2</sub> O <sub>3</sub>	Fe <sub>2</sub> O <sub>3</sub> <sup>*</sup>	MnO	MgO	CaO	Na <sub>2</sub> O	K <sub>2</sub> O	P <sub>2</sub> O <sub>5</sub>	LOI	Total	CaO/Al <sub>2</sub> O <sub>3</sub>
Ankaramites (high-Ca group)													
E4053 <sup>1</sup>	49.38	0.27	7.51	9.27	0.20	14.77	13.55	0.80	0.35	0.10	3.76	99.96	1.8
T4043 <sup>1</sup>	49.21	0.46	10.43	10.77	0.22	11.15	13.02	1.80	0.12	0.17	2.60	99.94	1.2
T4048 <sup>1</sup>	50.96	0.50	10.95	10.01	0.19	9.08	12.97	1.96	1.02	0.15	2.08	99.87	1.2
BIY-05-17 <sup>3</sup>	48.61	1.10	10.45	10.43	0.16	10.97	12.09	2.30	0.49	0.12	2.40	99.33	1.2
BIY-04-17 <sup>3</sup>	44.78	1.05	13.41	10.95	0.20	8.27	14.48	0.77	1.07	0.37	3.37	99.88	1.1
E4058 <sup>1</sup>	49.16	0.43	10.33	10.71	0.24	11.21	11.01	1.27	0.91	0.13	4.61	100.01	1.1
C-72Ж-04 <sup>2</sup>	49.93	0.46	11.31	11.18	0.18	9.33	12.04	1.14	1.24	0.13	2.77	99.70	1.1
E4048 <sup>1</sup>	48.68	0.40	11.77	9.52	0.18	11.58	12.19	1.41	0.67	0.14	3.14	99.68	1.0
T4051 <sup>1</sup>	50.44	0.52	12.68	10.37	0.19	7.98	12.19	1.50	0.98	0.19	2.90	99.94	1.0
Diopside popyry basalts (low-Ca group)													
BIY-01-02-17 <sup>3</sup>	46.37	1.00	15.80	9.74	0.16	7.03	11.86	1.78	1.63	0.12	3.68	99.53	0.8
BIY-07-15 <sup>3</sup>	45.87	1.16	13.97	13.52	0.22	7.94	9.82	2.20	1.30	0.19	3.21	99.63	0.7
BIY-08-15 <sup>3</sup>	47.09	1.00	14.61	12.04	0.19	7.80	9.47	2.23	2.72	0.18	2.52	100.07	0.6
BIY-02-15 <sup>3</sup>	46.74	1.17	16.23	10.42	0.18	7.31	10.28	2.14	0.69	0.17	3.87	99.57	0.6
BIY-03-15 <sup>3</sup>	45.51	1.16	16.86	11.86	0.18	7.67	9.43	1.64	1.78	0.17	3.24	99.76	0.6
BIY-06-17 <sup>3</sup>	47.02	1.03	17.71	11.08	0.14	6.00	9.61	2.83	1.06	0.20	2.71	99.51	0.5
BIY-06-15 <sup>3</sup>	47.36	1.24	17.49	11.12	0.21	6.01	8.32	2.28	0.84	0.13	4.23	99.53	0.5
BIY-05-15 <sup>3</sup>	45.17	0.95	16.38	12.64	0.19	8.44	7.61	3.04	0.80	0.19	4.23	100.01	0.5
BIY-04-15 <sup>3</sup>	47.89	1.23	17.58	8.61	0.18	8.26	8.13	2.62	1.47	0.23	3.49	99.95	0.5

Note. Analyses were carried out on a Thermo Scientific ARL-9900 XP spectrometer at V.S. Sobolev Institute of Geology and Mineralogy SB RAS, Novosibirsk. <sup>1</sup> (Gibsher et al., 1997); <sup>2</sup> (Safonova et al., 2011); <sup>3</sup> our data.

\* Total iron as Fe<sub>2</sub>O<sub>3</sub>.

clinopyroxene from the Katun' right-bank basalts (SiO<sub>2</sub> = 45.75–56.95, TiO<sub>2</sub> = 0.15–0.63, Na<sub>2</sub>O = 0.72–2.40, MgO = 7.76–14.08, and CaO/Al<sub>2</sub>O<sub>3</sub> = 1.0–1.9) (Fig. 5). In the TAS classification diagram, the composition points of the inclusions lie mostly in the field of basalts and are shifted to the field of basaltic andesites (Fig. 5a). In the CaO/Al<sub>2</sub>O<sub>3</sub> ratio (0.9–1.9) these inclusions are similar to the high-Ca basalts (CaO/Al<sub>2</sub>O<sub>3</sub> = 1.0–1.8) (Fig. 5b), but in the contents of most of rock-forming components (except for several inclusions from the Katun' right-bank samples) they overlap with both the high-Ca and the low-Ca basalts (Fig. 5).

#### THE CRITERIA FOR IDENTIFICATION OF ANKARAMITES AND THE GEODYNAMIC SETTINGS OF THEIR OCCURRENCE

The term ankaramite was first introduced by the French geologist Lacroix (1916) for the classification of basalt strata in the area of the Ankarami commune in the northwest of Madagascar. He proposed to use this term for rocks similar to picrites and associated with them but differing slightly in chemical composition and more significantly in mineral proportions (pyroxene dominates over olivine in ankaramites, and olivine dominates over pyroxene in picrites). According to these criteria, the Madagascar basalt formation was ac-

cepted as a petrotype of ankaramites (Gunn et al., 1970). Laz'ko and Sharkov (1988), taking into account the petrochemical composition of ankaramites, defined these rocks as subalkalic picrobasalts with low contents of MgO (15–17 wt.%). The Subcommittee on the Systematics of Igneous Rocks of the International Union of Geological Sciences (IUGS) decided that ankaramite is porphyritic melanocratic basanite with abundant pyroxene and olivine phenocrysts (Le Maitre et al., 2002). Further, it was established that ankaramites have CaO/Al<sub>2</sub>O<sub>3</sub> > 1 and the following mineral composition: high-Mg clinopyroxene, high-Mg olivine, Cr-spinel, and, rarely, high-Ca plagioclase (Frey et al., 1978; Ringwood, 1975; Della-Pasqua and Varne, 1997; Green et al., 2004).

Ankaramites occur in different geodynamic settings, which is well demonstrated by a tectonic schematic map with the marked sites of found ankaramites (Fig. 6). These rocks are present in the young island arcs of the Indian, Atlantic, and southwestern Pacific Oceans (Fig. 6), such as Vanuatu (Merelava and Epi Islands) (Barsdell, 1988; Barsdell and Berry, 1990), Sunda (Bali and Lombok Islands) (Della-Pasqua and Varne, 1997; Elburg et al., 2007), Lihir (Papua New Guinea) (Kennedy et al., 1990), and Nicaragua in the Costa Rica–Nicaragua segment of the Central American subduction zone (Carr and Rose, 1984). In these arcs, ankaramites are associated with rocks typical of island arc

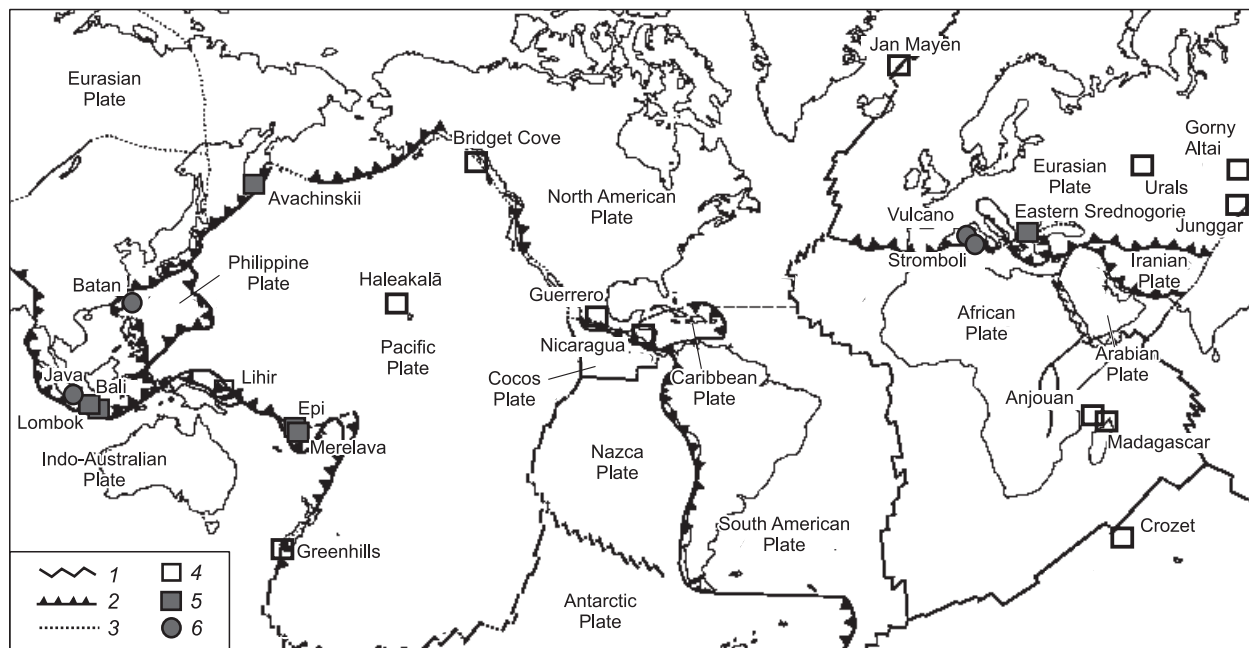


**Fig. 6.** Tectonic scheme of the occurrences of ankaramitic volcanism, after Schiano et al. (2000), modified and supplemented. 1–3, Plate boundaries: 1, mid-ocean ridge axes, 2, subduction zones, 3, transform faults; 4–6, occurrences of ankaramitic volcanism: 4, lavas, 5, lavas with high-Ca melt inclusions in olivine, 6, high-Ca melt inclusions in olivine.

systems, such as basaltic andesites, trachybasalts, trachyan-desites, and, more seldom, alkali basalts. Highly porphyritic olivine–clinopyroxene basalts and picrites were found on the isthmus of the Avachinskii Volcano on the southern margin of the Kamchatka arc eastern segment. These rocks are commonly described as avachites (Portnyagin et al., 2005a,b). By their specific features, they can be considered ankaramites.

In ancient island arcs, ankaramites were revealed in the form of dikes in the Greenhills Complex (New Zealand) (Mossman et al., 2000), as dikes and lava flows associated with trachyandesites and ultramafic–mafic intrusions of the Ural–Alaskan type in the South Urals (Medvedevka Formation) (Pushkarev et al., 2017), in association with picrites, basalts, and basaltic andesites in Junggar (northwestern China) (Zhang et al., 2008), in association with ultramafic–mafic intrusions of the Ural–Alaskan type in Alaska (Bridget Cove, Berners Bay) (Irvine, 1973), as lava flows associated with absarokites and shoshonites in Eastern Srednogorie (Bulgaria) (Marchev et al., 2009), and in association with ultramafic cumulates in Guerrero (Mexico) (Ortiz Hernández, 2000) (Fig. 6).

The Madagascar ankaramites associated with picrites (Lacroix, 1916), the Anjouan (Comores Archipelago) ankaramites associated with basalts, trachybasalts, and trachytes (Flower, 1973), the Haleakala (Maui Island, Hawaii) ankaramites associated with tholeiitic and alkali basalts (Hammer et al., 2016), and the Jan Mayen (north of Iceland) ankaramites associated with alkali basalts (Maaløe et al., 1986) appeared in intraplate settings. The East Island

(Crozet Archipelago, Indian Ocean) ankaramites associated with oceanites (Gunn et al., 1970) occur in mid-ocean ridge (MOR) zones (Fig. 6).

Melt inclusions with  $\text{CaO}/\text{Al}_2\text{O}_3 > 1$  were found in high-Mg olivine from ankaramites of the Vanuatu and Sunda arcs (Della-Pasqua and Varne, 1997), from avachites (ankaramites) of the Avachinskii Volcano (Portnyagin et al., 2005a,b), and from calc-alkaline basalts of Batan (Luzon–Taiwan Arc) (Schiano et al., 2000), Java (Sunda Arc) (Sisson and Bronto, 1998), and Vulcano and Stromboli (Aeolian Arc, Italy) islands (Gioncada et al., 1998) (Fig. 6). Melt inclusions with  $\text{CaO}/\text{Al}_2\text{O}_3 > 1$  were also found in high-Mg clinopyroxene from ankaramites of the Vanuatu and Sunda arcs (Della-Pasqua and Varne, 1997) and from diopside porphyry basalts of the Ust’-Sema Formation (Buslov et al., 1993; Simonov et al., 2010). The analysis of the localization of ankaramites shows that high-Ca volcanism is possible in both subduction and intraplate settings. It is occurred along with suprasubductional or intraplate magmatism.

## THE MINERAL AND PETROGRAPHIC FEATURES OF THE ANKARAMITES

To establish the mineral and petrographic features of the ankaramites, we used data on the well-studied ankaramites of different island arc systems (Barsdell and Berry, 1990; Della-Pasqua, 1997; Ortiz Hernández, 2000; Zhang et al., 2008; Marchev et al., 2009; Pushkarev et al., 2017) and on avachites (Portnyagin et al., 2005a) as well as our data on

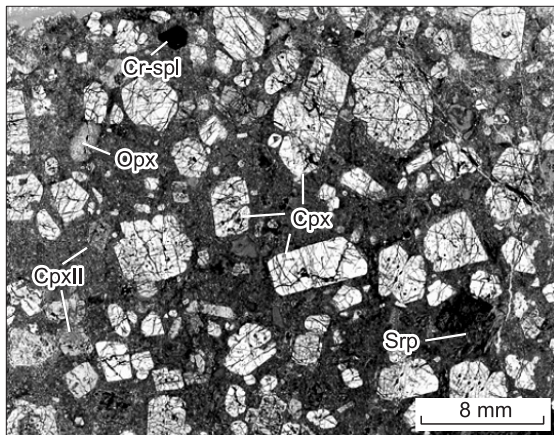


**Fig. 7.** Photomicrograph of the South Urals ankaramites (Pushkarev et al., 2018). Cpx, Cr-diopside phenocrysts, Cpx II, fine diopside phenocrysts, Opx, chlorite pseudomorphs after olivine (or orthopyroxene) phenocrysts, Cr-spl, Cr-spinel phenocrysts, Srp, serpentinite microxenolith.

the high-Ca diopside porphyry basalts of the Ust'-Sema Formation.

Ankaramites have a porphyritic texture and contain phenocrysts of high-Mg clinopyroxene, high-Mg olivine, and, more seldom, plagioclase and Cr-spinel. The microlitic groundmass is composed of clinopyroxene and plagioclase (Fig. 7).

**Clinopyroxene** is present as phenocrysts and microlites in the groundmass. The total content of the phenocrysts is usually >25 vol.% (up to 70 vol.%). These are large (up to 4 cm; on average, 1–6 mm) euhedral crystals (Figs. 2a, 3a, d, and 7). Most of the phenocrysts have a normal zoning (Fig. 3a, d); the phenocrysts with a reverse zoning are scarce. The Mg# value varies from 75 to 94 in the cores of the phenocrysts and decreases to 53 in the rims (Fig. 8). The clinopyroxene is represented by diopside and augite (Fig. 8f). The Mg# values show a negative correlation with the TiO<sub>2</sub>, Al<sub>2</sub>O<sub>3</sub>, and Na<sub>2</sub>O contents and a positive correlation with the Cr<sub>2</sub>O<sub>3</sub>, CaO, and SiO<sub>2</sub> contents, which is typical of the general evolution trend of clinopyroxene composition during the crystallization of primitive basaltic magmas (Fig. 8a–e). The Al<sub>2</sub>O<sub>3</sub> content varies from 0.5 to 5.0 wt.%, reaching 9 wt.% in clinopyroxenes from Eastern Srednogie and the Ust'-Sema Formation (Fig. 8b). The lowest contents of Al<sub>2</sub>O<sub>3</sub> (<3 wt.%) are found in clinopyroxenes from the Urals and Junggar ankaramites (Fig. 8b). The same tendency is observed for TiO<sub>2</sub> and Na<sub>2</sub>O (Fig. 8a, e). A specific feature of the clinopyroxenes from ankaramites is high Mg# and Cr# values (Fig. 8d). The Cr<sub>2</sub>O<sub>3</sub> content reaches 1.1 wt.%, which permits us to classify the mineral as chromian diopside (Fig. 8d).

**The amount of olivine** phenocrysts varies from 3 to 31 vol.% but does not exceed the amount of clinopyroxene. Note that ankaramites of ancient island arc systems, e.g., the South Urals, East Srednogie, and Junggar ones (Figs. 2d

and 7), often contain olivine phenocrysts totally replaced by secondary products. The composition of olivine was studied in ankaramites from young island arcs (Vanuatu and Sunda) and in Kamchatkan avachites. Olivine has skeletal, rounded, and euhedral crystals 1–6 mm (seldom, up to 20 mm) in size and shows a wide variation in composition (Fo<sub>75–92</sub>). The crystals are usually of homogeneous composition but sometimes have a reverse zoning. Olivine has high contents of CaO (0.10–0.55 wt.%) and medium contents of NiO (up to 0.3 wt.%). The latter is in positive correlation with the forsterite component. Olivine Fo<sub>>85</sub> often contains melt inclusions. Their examination led to a conclusion about the existence of high-Ca ankaramitic melts (CaO/Al<sub>2</sub>O<sub>3</sub> > 1).

**Plagioclase** phenocrysts are scarce (<1 vol.%) and small (<1 mm). This mineral is present mostly as microlites in the groundmass (Fig. 2e). The phenocrysts have a composition An<sub>49–93</sub> (Fig. 2e, Table 2). The most mafic ankaramites (e.g., South Urals ones) lack plagioclase. The groundmass of the most primitive ankaramites can contain microlites with a composition An<sub>90</sub> (Barsdell, 1988).

**Cr-spinel** phenocrysts are scarce. This mineral is usually found as inclusions in phenocrysts of high-Mg olivine or high-Mg clinopyroxene. The Cr# value varies mostly from 50 to 90 and is sometimes <10 (Fig. 9b). The Mg# value is within 30–70, reaching 80 in low-Cr ankaramites (Fig. 9b). It is not ruled out that Cr-spinels of this composition can be xenogenic. The Al<sub>2</sub>O<sub>3</sub>–TiO<sub>2</sub> diagram shows that most of the studied Cr-spinels fall in the field of typical island arc basalts (Fig. 9a).

**The groundmass** is microlitic and consists of predominant clinopyroxene (diopside–augite and, sometimes, pigeonite) and subordinate plagioclase An<sub>70–94</sub>, titanomagnetite, and/or olivine (iron-rich varieties Fo<sub>43–49</sub>).

## THE PETROCHEMICAL FEATURES OF THE ANKARAMITES

To elucidate the petrochemical features of the ankaramites, we used the data on ankaramites of typical island arc systems, on their petrotype (Mt. Ankarami, Madagascar) (Table 6), and on homogenized high-Ca melt inclusions in olivine from ankaramites and basalts (Tables 1, 2 (Schiano et al., 2000), and 3 (Portnyagin et al., 2005b)).

The SiO<sub>2</sub> and MgO contents in the considered ankaramites are within 43.27–51.74 and 7.98–18.44 wt.%, respectively. In the TAS classification diagram for high-Mg volcanics, the composition points of these rocks are in the fields of basalts and, more seldom, picobasalts (Fig. 10a, Table 6). The high-Ca ankaramites of the Ust'-Sema Formation are also in the fields of basalts and, more seldom, picobasalts (Fig. 10a). The Vanuatu, South Urals, Junggar, and Avachinskii Volcano ankaramites and the high-Ca ankaramites of the Ust'-Sema Formation belong to the subalkaline series, whereas the Sunda Arc, East Srednogie, and Madagascar ankaramites, to the alkaline series (Fig. 10a).

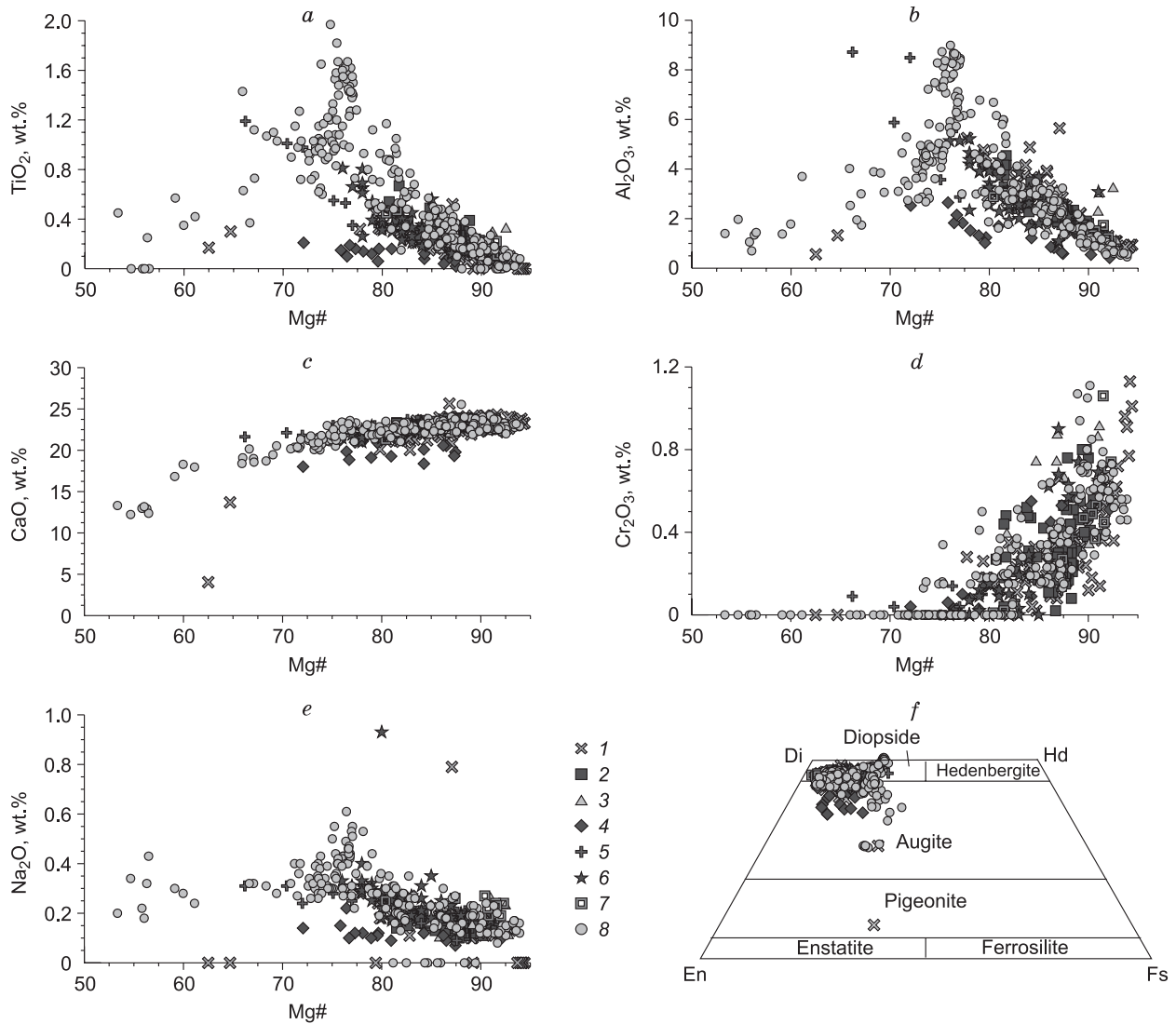


**Fig. 8.** Compositional variations (a–e) and classification (Morimoto, 1988) ( $\bar{X}$ ) of clinopyroxenes from ankaramites. 1–6, Ankaramites: 1, Vanuatu Arc (Barsdell and Berry, 1990; Della-Pasqua, 1997), 2, Sunda Arc (Della-Pasqua, 1997), 3, Junggar (Zhang et al., 2008), 4, South Urals (Pushkarev et al., 2017), 5, Eastern Srednogie (Marchev et al., 2009), 6, Guerrero (Ortiz Hernández, 2000); 7, avachites, Kamchatka (Portnyagin et al., 2005a); 8, high-Ca group of diopside porphyry basalts of the Ust'-Sema Formation.

The composition points of homogenized high-Ca melt inclusions in olivine from ankaramites, basalts, and avachites lie in the fields of basalts, being shifted to the field of basanites and tephrites (Fig. 10a). Similar melt inclusions in clinopyroxene from basalts of the Ust'-Sema Formation fall in the field of subalkaline series; their SiO<sub>2</sub> content reaches 57 wt.% (Fig. 10a).

Two types of high-Ca melts were recognized by a detailed study of the homogenized high-Ca melt inclusions in ankaramites and basalts from different occurrences (Schiano et al., 2000; Kogiso and Hirschmann, 2001): (1) hypersthene-normative, saturated with SiO<sub>2</sub> and undersaturated with K, in MOR zones, back-arc basins, and oceanic islands and (2) nepheline-normative, undersaturated with SiO<sub>2</sub> and saturated with K, in island arc (shoshonite) series.

In the classification diagrams, the considered ankaramites show wide variations in the contents (wt.%) of CaO (8.82–21.12), Al<sub>2</sub>O<sub>3</sub> (6.02–13.80), and FeO (6.15–11.13) and narrow variations in the contents of TiO<sub>2</sub> (0.13–1.10) (and up to 3 wt.% in the Madagascar ankaramites), Na<sub>2</sub>O (0.07–2.30), and K<sub>2</sub>O (0.01–1.85) (Fig. 10b–g, Table 6). Homogenized high-Ca melt inclusions in olivine and clinopyroxene have low contents (wt.%) of MgO (4.39–15.85) and CaO (11.30–18.70) and high contents of Al<sub>2</sub>O<sub>3</sub> (6.99–14.23), TiO<sub>2</sub> (0.15–1.28), Na<sub>2</sub>O (0.72–3.49), and K<sub>2</sub>O (0.54–2.12) (Fig. 10 b–g). They differ considerably from the ankaramites in the contents of FeO and SiO<sub>2</sub> (Fig. 10f, g).

The composition of homogenized melt inclusions in early minerals of ankaramites can differ from the composition of trapped melt portions (Danyushevsky et al., 2002; Portnyagin et al., 2005a).

**Table 6.** Representative analyses (wt.%) of ankaramites from different occurrences

Locality	Reference	SiO <sub>2</sub>	TiO <sub>2</sub>	Al <sub>2</sub> O <sub>3</sub>	FeO*	MnO	MgO	CaO	Na <sub>2</sub> O	K <sub>2</sub> O	P <sub>2</sub> O <sub>5</sub>	LOI	Total	CaO/ Al <sub>2</sub> O <sub>3</sub>
Madagascar	(Lacroix, 1916)	45.84	3.00	7.45	11.13	—	16.76	12.64	1.38	0.99	0.42	0.42	100.20	1.7
Madagascar	(Lacroix, 1916)	43.27	1.25	7.54	8.27	—	17.65	13.72	1.26	1.14	0.38	4.54	100.54	1.8
Junggar, China	(Zhang et al., 2008)	50.66	0.50	9.51	9.33	0.21	16.64	10.03	1.64	0.84	0.26	5.45	99.62	1.1
Junggar, China	(Zhang et al., 2008)	49.65	0.49	10.25	10.19	0.19	15.74	9.86	1.67	1.23	0.24	3.91	99.51	1.0
Junggar, China	(Zhang et al., 2008)	49.72	0.48	9.84	10.54	0.20	15.46	10.24	1.90	0.86	0.24	4.01	99.48	1.0
Junggar, China	(Zhang et al., 2008)	50.89	0.46	9.92	10.27	0.23	14.75	9.76	2.07	0.99	0.25	4.35	99.59	1.0
Junggar, China	(Zhang et al., 2008)	50.54	0.41	8.96	10.33	0.20	17.54	9.14	0.48	1.85	0.24	5.54	99.69	1.0
Junggar, China	(Zhang et al., 2008)	51.74	0.41	8.39	9.34	0.21	18.05	8.82	1.22	1.27	0.24	4.97	99.69	1.1
Merelava, Vanuatu	(Della-Pasqua and Varne, 1997)	51.33	0.59	13.10	8.20	0.22	10.67	12.45	1.78	0.35	0.07	0.62	98.76	1.0
Merelava, Vanuatu	(Della-Pasqua and Varne, 1997)	50.20	0.46	10.30	8.08	0.17	13.71	13.69	1.60	0.38	0.05	0.90	98.64	1.3
Epi, Vanuatu	(Barsdell and Berry, 1990)	48.20	0.45	13.80	9.72	0.17	10.50	14.20	1.26	0.37	0.07	0.10	99.92	1.0
Epi, Vanuatu	(Barsdell and Berry, 1990)	47.80	0.43	13.60	9.54	0.18	10.70	14.20	1.29	0.35	0.09	0.31	99.55	1.0
Epi, Vanuatu	(Della-Pasqua and Varne, 1997)	48.20	0.39	11.50	8.91	0.16	13.50	14.40	1.05	0.31	0.07	0.10	98.49	1.3
Rinjani, Sunda Arc	(Della-Pasqua and Varne, 1997)	47.95	0.83	13.78	10.16	0.17	10.61	13.14	1.78	1.20	0.21	—	99.83	1.0
Rinjani, Sunda Arc	(Della-Pasqua and Varne, 1997)	48.32	0.69	10.53	9.19	0.17	14.02	14.38	1.50	0.90	0.15	—	99.85	1.4
Ulakan, Sunda Arc	(Della-Pasqua and Varne, 1997)	46.44	0.56	9.12	10.30	0.20	17.48	11.78	1.22	0.61	0.21	0.41	97.92	1.3
Ulakan, Sunda Arc	(Della-Pasqua and Varne, 1997)	46.86	0.79	11.84	10.20	0.19	13.30	11.84	1.59	0.94	0.28	0.42	97.83	1.0
Sakmara–Voznesenka zone, South Urals	(Pushkarev et al., 2017)	46.14	0.18	7.01	8.58	0.24	16.60	17.08	0.11	0.01	0.13	3.50	99.97	2.4
Sakmara–Voznesenka zone, South Urals	(Pushkarev et al., 2017)	45.43	0.17	6.60	8.47	0.20	17.70	16.79	0.10	0.01	0.11	3.70	99.75	2.5
Sakmara–Voznesenka zone, South Urals	(Pushkarev et al., 2017)	46.08	0.16	6.02	8.37	0.19	18.44	16.50	0.10	0.04	0.12	3.40	99.94	2.7
Sakmara–Voznesenka zone, South Urals	(Pushkarev et al., 2017)	43.89	0.15	6.24	8.15	0.29	17.68	20.01	0.07	0.00	0.12	3.10	100.30	3.2
Sakmara–Voznesenka zone, South Urals	(Pushkarev et al., 2017)	46.32	0.13	6.36	7.70	0.20	15.05	21.12	0.18	0.02	0.06	2.50	100.04	3.3

Note. Dash, analysis for the component was not performed or its content is below the detection limit.

\*Total iron as FeO.

gin et al., 2005b). Melt inclusions trapped during the crystallization of primitive magmas can undergo re-equilibration with the host mineral, partial crystallization, and decrepitation under decompression (Portnyagin et al., 2005b), with

the loss of the fluid components (CO<sub>2</sub> and H<sub>2</sub>O) and part of the residual silicate melt (Danyushevsky et al., 2002; Portnyagin et al., 2005b). The primitive melts of the inclusions in olivine are richer in Al<sub>2</sub>O<sub>3</sub>, Na<sub>2</sub>O, and K<sub>2</sub>O and poorer in

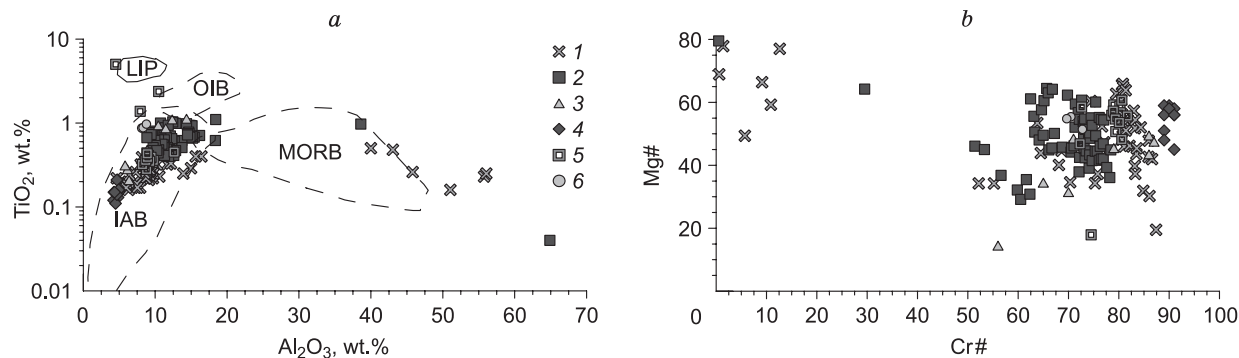


**Fig. 9.** Compositional variations of Cr-spinel from ankaramites. *a*, Variations in the Al<sub>2</sub>O<sub>3</sub> and TiO<sub>2</sub> contents depending on geodynamic setting (Kamenetsky et al., 2001); *b*, variations in Cr# = 100·Cr/(Cr + Al) and Mg# = 100·Mg/(Mg + Fe<sup>2+</sup>). 1–4, ankaramites: 1, Vanuatu Arc (Barsdell and Berry, 1990; Della-Pasqua, 1997), 2, Sunda Arc (Della-Pasqua, 1997), 3, Junggar (Zhang et al., 2008), 4, South Urals (Pushkarev et al., 2017); 5, avachites, Kamchatka (Portnyagin et al., 2005a); 6, high-Ca group of diopside porphyry basalts of the Ust'-Sema Formation. IAB, island arc basalts; OIB, ocean island basalts; MORB, mid-ocean ridge basalts; LIP, large igneous provinces.

SiO<sub>2</sub> than the rocks (Fig. 10). Taking into account this fact, Portnyagin et al. (2005b) proposed a technique for studying melt inclusions in olivine from ankaramites (avachites).

A specific petrochemical feature of both the ankaramites and the high-Ca melt inclusions in their olivine and clinopyroxene is CaO/Al<sub>2</sub>O<sub>3</sub> > 1, which is much higher than CaO/Al<sub>2</sub>O<sub>3</sub> = 0.8–0.9 in the upper-mantle melts and in typical picrites (Fig. 10b, Table 6) (Frey et al., 1978; Ringwood, 1975; Della-Pasqua and Varne, 1997; Green et al., 2004). The Urals ankaramites have lower contents of Al<sub>2</sub>O<sub>3</sub> (<7 wt.%) and TiO<sub>2</sub> (<0.2 wt.%), a higher content of CaO (>16 wt.%), and a higher CaO/Al<sub>2</sub>O<sub>3</sub> ratio (up to 3.3) as compared with other typical ankaramites of the Vanuatu and Sunda arcs (Fig. 10b–e). The high-Ca basalts of the Ust'-Sema Formation are similar in the contents of all major components to typical ankaramites (Fig. 10). The homogenized high-Ca melt inclusions in clinopyroxene from these basalts are also similar in CaO/Al<sub>2</sub>O<sub>3</sub> and the contents of major components to ankaramites (Fig. 10).

## DISCUSSION

The abundance of high-Mg clinopyroxene phenocrysts (>25 vol.%, Mg# ≤ 94), the high Cr# values (up to 91), and the high-Ca plagioclase (An<sub>49–93</sub>) are typical of the ankaramites and associated high-Ca basalts of the Ust'-Sema Formation (Figs. 2a, e, 4, 7, and 9, Table 2). The evolution of the composition of clinopyroxene from the Ust'-Sema basalts and its variations are also specific to island arc ankaramites, e.g., the Vanuatu and Sunda ones (Figs. 4 and 8). However, this clinopyroxene has higher contents of TiO<sub>2</sub> and Al<sub>2</sub>O<sub>3</sub> than those from the Urals and Junggar ankaramites and Kamchatka avachites (Figs. 4a, b and 8a, b). Thus, the high-Ca basalts of the Ust'-Sema Formation can be assigned to ankaramites according to their mineralogical and petrographic features. The content of clinopyroxene phenocrysts in the low-Ca basalts is much lower because of the increase in the amount of plagioclase, although they contain high-Mg clinopyroxene and are characterized by specific variations in its composition and high Cr# values of Cr-spinel, which is typical of ankaramites.

According to the petrochemical data, ankaramites are characterized by a high CaO/Al<sub>2</sub>O<sub>3</sub> ratio (>1), which is also established in the high-Ca basalts of the Ust'-Sema Formation. The homogenized melt inclusions in clinopyroxene phenocrysts from these basalts also have CaO/Al<sub>2</sub>O<sub>3</sub> > 1 (Buslov et al., 1993; Simonov et al., 2010). Thus, the Ust'-Sema high-Ca basalts are ankaramites according to their mineralogical, petrographic, and petrochemical features. During the crystallization of ankaramites, the composition of clinopyroxene evolves toward an increase in the Fe/(Fe + Mg) value and Al, Ti, and Na contents and a decrease in the Cr content. This suggests that the low-Ca basalts of the Ust'-Sema Formation resulted from the fractionation of an-

karamitic melt in intermediate magma chambers, which does not rule out enrichment of some basalt flows with cumulus clinopyroxene (Figs. 4 and 8).

The above classifications of the ankaramites and low-Ca basalts of the Ust'-Sema Formation according to their mineralogical, petrographic, and petrochemical features are based on the earlier recommendations (Le Maitre et al., 2002) and permit defining ankaramites as subalkaline high-Mg olivine-clinopyroxene basalts with CaO/Al<sub>2</sub>O<sub>3</sub> > 1.

In mineral and chemical compositions, the Gorny Altai ankaramites are most similar to island arc ankaramites. At the same time, the basalts of the Ust'-Sema Formation in the the Biika volcanic edifice are associated with the underlying Manzherok Formation composed of rocks with intraplate geochemical characteristics (Safonova et al., 2011). In fact, the Ust'-Sema volcanics overbuild (with a time gap) the volcanic edifice of the Manzherok Formation and overlies the carbonates of the Cheposh Formation. The dual nature of the Ust'-Sema Formation basalts makes it necessary to consider the models of generation of high-Ca melts producing ankaramites.

Some researchers interpreted the high-Ca composition of ankaramites as the result of accumulation of clinopyroxene crystals from picritic or olivine basaltic magmas (Gunn et al., 1970; Hughes, 1982). Others stated the existence of primary ankaramitic magmas (Thompson and Flower 1971; Maaløe et al., 1986; Barsdell and Berry 1990; Della Pasqua and Varne, 1997; Schiano et al., 2000). Before the findings of melt inclusions of ankaramitic composition, a series of experiments on the partial melting of various substrates was carried out for explaining and confirming the existence of primary ankaramitic melts: (1) Experiments at low pressure (1 bar) showed that ankaramites can form not through the accumulation of clinopyroxene from basaltic melts but through the prolonged equilibrium crystallization of magma at 1240–1275 °C (Thompson and Flower, 1971). (2) Experiments at 19.5 kbar and 1415 °C demonstrated that ankaramites can form at the low degree of partial melting of spinel lherzolite (Maaløe et al., 1986). (3) Experiments at 5–10 kbar and 1325 °C confirmed that ankaramitic melts can be produced from wehrlites or clinopyroxenites (Barsdell and Berry, 1990).

Homogenization of high-Ca melt inclusions in high-Mg olivine from the ankaramites of the Vanuatu and Sunda arcs proves the existence of high-Ca (ankaramitic) melts differing significantly from picritic ones (Della Pasqua and Varne, 1997). The mentioned researchers believe that these high-Ca melts cannot be produced through the partial melting of "pure" mantle lherzolites but can form during the partial melting of lherzolite in the presence of CO<sub>2</sub>-enriched fluids at 10–30 kbar. Based on the results of study of high-Ca melt inclusions in olivine from the calc-alkaline basalt of Batan Island, Schiano et al. (2000) recognized a special type of primitive nepheline-normative ankaramitic island arc magma and proposed a model for the formation of these inclu-

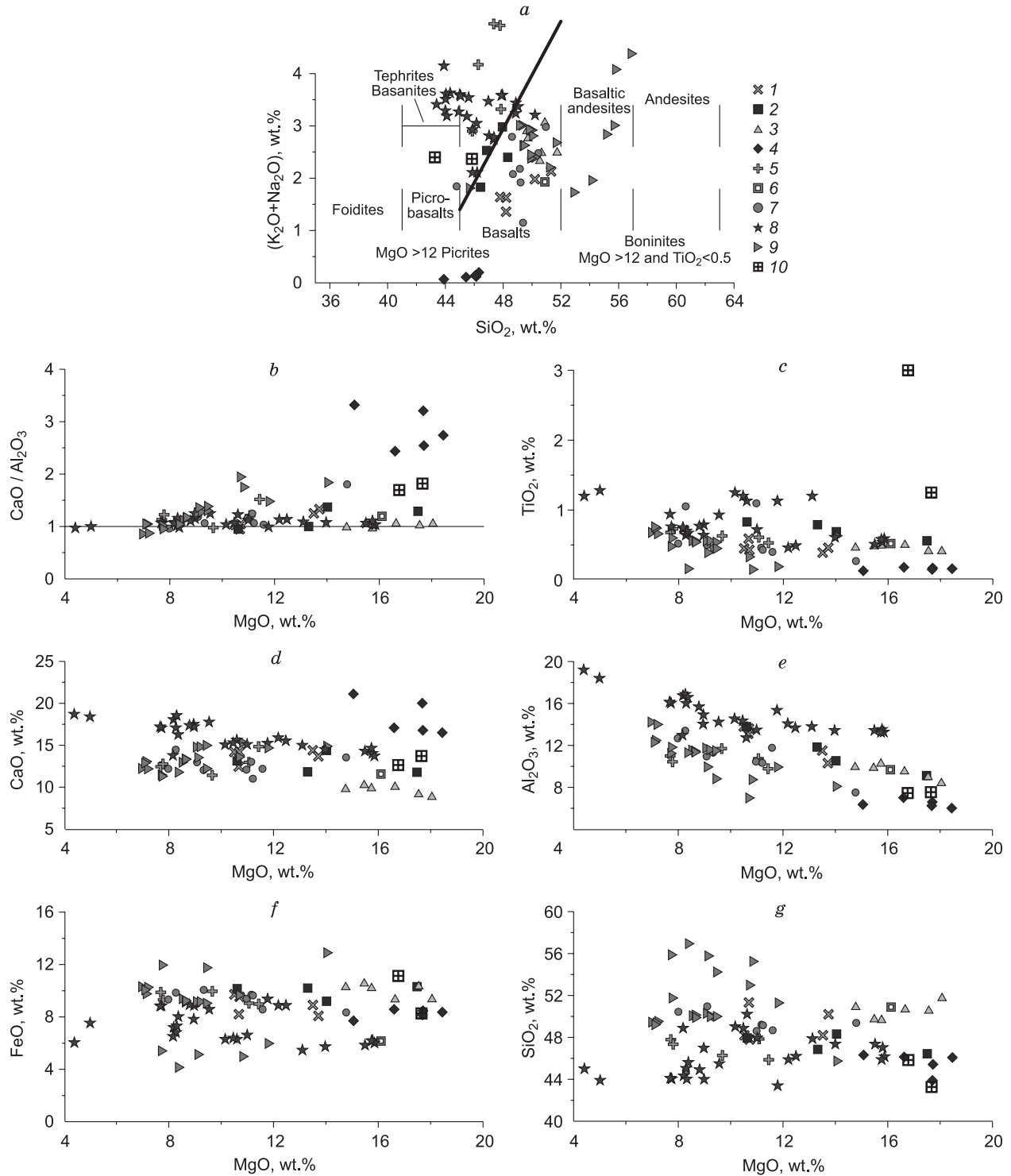


**Fig. 10.** Classification and compositional variations of ankaramites and high-Ca melt inclusions. *a* — TAS classification diagram for high-Mg volcanics (Le Maitre et al., 2002), bold line marks the boundary between subalkaline and alkali basalts (Le Maitre et al., 2002); *b–g*, variations in composition. 1–5, ankaramites: 1, Vanuatu Arc (Barsdell and Berry, 1990; Della-Pasqua and Varne, 1997), 2, Sunda Arc (Della-Pasqua and Varne, 1997), 3, Junggar (Zhang et al., 2008), 4, South Urals (Pushkarev et al., 2017), 5, Eastern Srednogorie (Marchev et al., 2009); 6, avachites, Kamchatka (average composition) (Portnyagin et al., 2005a); 7, high-Ca group of the basalts of the Ust'-Sema Formation, Gorny Altai (Gibsher et al., 1997; Safonova et al., 2011); our data); 8, 9, homogenized high-Ca melt inclusions: 8, in olivine from ankaramites, basalts, and avachites (Schiano et al., 2000; Portnyagin et al., 2005b), 9, in clinopyroxene from the basalts of the Ust'-Sema Formation (Buslov et al., 1993; Simonov et al., 2010); 10, ankaramites of Madagascar (Lacroix, 1916).

sions during the medium- and high-degree partial melting of pyroxenite cumulates (~10–40 wt.%) at the lower-crust–upper-mantle pressures. Thus, two types of high-Ca ankaramitic magmas are recognized: hypersthene-normative and nepheline-normative, which might have different mechanisms of formation.

As mentioned above, the composition of homogenized high-Ca melt inclusions in high-Mg olivine or high-Mg clinopyroxene in ankaramites or basalts differs from the bulk composition of ankaramites (Danyushevsky et al., 2002; Portnyagin et al., 2005b). In the further research we will discuss these phenomena and consider the application of new techniques to study melt inclusions in the rocks of the Ust'-Sema Formation and ankaramites.

Hypersthene-normative high-Ca melts can form in the following ways: (1) during the partial melting of clinopyroxenite (at >1350 °C and 10 kbar) accompanied by a reaction between the melt and the rock (Kamenetsky et al., 1998; Kogiso and Hirschmann, 2001); (2) during the melting of a refractory olivine + clinopyroxene ± orthopyroxene source at elevated mantle temperatures. (at least 1350–1400 °C) and a pressure of 12 kbar (Médard et al., 2004); (3) from a refractory lherzolitic source enriched in CaO; such a source is readily produced from fertile lherzolite (1300–1350 °C) by first-stage melt extraction and subsequent enrichment with dolomitic carbonatite melt, which increases the CaO and Na<sub>2</sub>O contents and the modal amount of diopside without increasing the Al<sub>2</sub>O<sub>3</sub> content; (4) from a lherzolitic source, leaving residual refractory clinopyroxene-bearing or clinopyroxene-free harzburgite (Schmidt et al., 2004) at 15 kbar and 1300–1360 °C in the presence of H<sub>2</sub>O and CO<sub>2</sub> or at >1400 °C in anhydrous conditions. The main problem in the models for the formation of such melts is the high temperature (>1350 °C) required for melting, whereas the estimated temperatures beneath typical MORs are ~1280–1350 °C (White et al., 1992) and the temperatures in the mantle wedge are even lower, ~1100 °C (England and Wilkins, 2004).

Nepheline-normative high-Ca melts cannot be produced through the partial melting of typical mantle lherzolite. The following models of their formation were proposed: (1) partial melting of amphibole-containing wehrlite at low temperatures (>1190 °C), 10 kbar, and the low degrees of partial melting (Médard et al., 2006); (2) formation from a metasomatized garnet-free mantle source consisting of clinopyroxene and olivine (wehrlite) and containing either amphibole or jadeite (Elburg et al., 2007); and (3) formation from amphibole-containing clinopyroxenites present as cumulates in the lower crust and/or as metasomatic veins in the island-arc-related upper mantle (Sorbadere et al., 2013). Amphibole is considered an important phase for the formation of nepheline-normative ankaramites for two reasons. First, the water present in it significantly decreases the temperature of clinopyroxenite melting to the values typical of island arc settings (Schiano et al., 2000; Médard et al., 2006). Second, the melting of amphibole also contributes to an increase in the amount of alkalis and to a decrease in SiO<sub>2</sub> content as

compared with pure clinopyroxenite and wehrlite melts, and the produced melts are shifted by composition to nepheline-normative magmas (Sorbadere et al., 2013).

The above review of the ankaramite genesis models shows that ankaramitic melt cannot form directly from lherzolites. It can be produced either through the mantle wehrlitization or through the melting of wehrlites or clinopyroxenites present in the mantle or lower crust. Carbonates in subduction zones serve as wehrlitization agents for island arc ankaramites, and carbonatites related to deep-seated mantle plumes, as the same agents for intraplate ankaramites. It is not quite clear what caused wehrlitization of the mantle that produced the ankaramites of the Ust'-Sema Formation. According to Safonova et al., (2011) and Simonov et al., (2010), the Ust'-Sema diopside porphyry basalts resulted from subduction processes. In this case, wehrlitization of the mantle might have been caused by the pull of carbonates into the subduction zone. This model is supported by the fact that similar volcanics and dikes form an extended linear belt (Izokh et al., 2004). There are also middle Cambrian intraplate carbonatites in Gorny Altai that might have caused wehrlitization of the local lithospheric mantle at the same time (Vrublevskii et al., 2012). The geodynamic setting of effusion of the Gorny Altai ankaramites and the sources of their primary melts call for further study.

## CONCLUSIONS

The genesis of mafic magmatism during the Neoproterozoic–early Paleozoic stage of evolution of the Altai–Sayan folded area, in particular, of middle Cambrian diopside porphyry basalts of the Ust'-Sema Formation in Gorny Altai (Buslov et al., 1993, 2001; Gibsher et al., 1997; Dobretsov et al., 2004; Zybin, 2006; Simonov et al., 2010; Safonova et al., 2011), is a controversial issue. These rocks contain numerous phenocrysts of high-Mg (Mg# ≤ 94) clinopyroxene (20–50 vol.%). In addition, there are phenocrysts of saussuritized plagioclase (An<sub>49–71</sub>), olivine completely replaced by an aggregate of chlorite, epidote, and amphibole, and, more seldom, amphibole with Mg# = 55.7–68.2 and Cr-spinel with Cr# = 36.2–41.7. Cr-spinel inclusions in the high-Mg clinopyroxene are characterized by high Cr# values (up to 72.8). The basalts of the Ust'-Sema Formation are subdivided into two main groups according to chemical composition: high-Ca (CaO = 11.01–14.48 wt.%, MgO = 7.98–14.77 wt.%, and CaO/Al<sub>2</sub>O<sub>3</sub> = 1.0–1.8). Comparison of the studied Ust'-Sema high-Ca basalts with the reviewed ankaramites gives grounds to assign them to this type of rocks. Based on the recommendations by Le Maitre et al. (2002), we performed a detailed classification analysis of ankaramites with regard to their mineralogical, petrographic, and petrochemical features. The results permit us to define ankaramites as subalkaline high-Mg olivine–clinopyroxene basalts with CaO/Al<sub>2</sub>O<sub>3</sub> > 1. The low-Ca basalts of the Ust'-Sema Formation probably resulted from the fractionation of ankaramitic melt in intermediate magma chambers. The

Gorny Altai ankaramites formed through the melting of the wehrlitized suprasubductional lithospheric mantle of the Central Asian Orogenic Belt.

The ankaramitic magmatism of the Ust'-Sema Formation and the comagmatic ultramafic–mafic intrusions of the Barangol complex suggest the existence of intrusions similar to the massifs of the Ural–Alaskan type in the Altai–Sayan folded area. During the crystallization of ankaramites, the composition of clinopyroxene evolves toward an increase in the Fe/(Fe + Mg) values and Al, Ti, and Na contents and a decrease in the Cr content. This evolution trend is controlled by the olivine–clinopyroxene cotectic fractionation and is typical of both island arc ankaramites (Irvine, 1973; Barsdell and Berry, 1990; Della-Pasqua and Varne, 1997; Mossman et al., 2000) and ultramafic rocks of Ural–Alaskan type complexes (Irvine, 1973; Pushkarev et al., 2017). Ankaramitic melts can be generated from a mantle source with a high CaO/Al<sub>2</sub>O<sub>3</sub> ratio exceeding that in the lherzolitic (pyrolytic) mantle. This composition is specific to wehrlites, which are usually not characteristic of the mantle. The metasomatized wehrlitic mantle can result either from the reaction of lherzolite with mantle carbonatitic melts or from the interaction of mantle wedge rocks with fluid components of the subducting slab. Experiments aimed at elucidating the genesis of ankaramites showed that one of the most probable mechanisms of their formation is the melting of wehrlites or clinopyroxenites in the upper mantle of island arcs with the participation of amphibole (Médard et al., 2006; Sorbadere et al., 2013).

We thank the reviewers V.A. Simonov and P.Yu. Plechov for valuable critical remarks, which helped to improve the paper, I.Yu. Safonova and A.S. Gibsher for the consultation on the objects of previous studies, and A.I. Il'in, E.V. Mikheev, and D.V. Elkina for the participation in the field studies.

The work is done on state assignment of IGM SB RAS with a financial support by project 14.Y26.31.0018 from the Ministry of Education and Science of the Russian Federation.

## REFERENCES

- Barsdell, M., 1988. Petrology and petrogenesis of clinopyroxene-rich olivine tholeiitic lavas from Merelava Volcano, Vanuatu. *J. Petrol.* 29, 927–964.
- Barsdell, M., Berry, R.F., 1990. Origin and evolution of primitive island arc ankaramites from Western Epi, Vanuatu. *J. Petrol.* 31, 747–777.
- Buslov, M.M., Bersin, N.A., Dobretsov, N.L., 1993. Geology and tectonics of Gorny Altai. Guide-book for post-symposium excursion. The 4th International Symposium of the IGCP Project 283 “Geodynamic Evolution of the Paleoasian Ocean”. UIGGM SB RAS, Novosibirsk.
- Buslov, M.M., Safonova, I.Yu., Watanabe, T., Obut, O.T., Fujiwara, Y., Iwata, K., Semakov, N.N., Sugai, Y., Smirnova, L.V., Kazansky, A.Yu., Itaya, T., 2001. Evolution of the Paleo-Asian Ocean (Altai–Sayan Region, Central Asia) and collision of possible Gondwana-derived terranes with the southern marginal part of the Siberian continent. *Geosci. J.* 5 (3), 203–224.
- Carr, M.J., Rose, W.I., 1984. A data base of Central American volcanic rocks. *J. Volcanol. Geotherm. Res.* 33, 239–240.
- Danyushevsky, L.V., McNeill, A.W., Sobolev, A.V., 2002. Experimental and petrological studies of melt inclusions in phenocrysts from mantle-derived magmas: An overview of techniques, advantages and complications. *Chem. Geol.* 183, 5–24.
- Della-Pasqua, F.N., 1997. Primitive ankaramitic magmas in volcanic arcs: evidence from melt inclusions. PhD Thesis. University of Tasmania.
- Della-Pasqua, F.N., Varne, R., 1997. Primitive ankaramitic magmas in volcanic arcs: A melt inclusion approach. *Can. Mineral.* 35, 291–312.
- Dobretsov, N.L., Buslov, M.M., Safonova, I.Yu., Kokh, D.A., 2004. Fragments of oceanic islands in the Kurai and Katun' accretionary wedges of Gorny Altai. *Geologiya i Geofizika (Russian Geology and Geophysics)* 45 (12), 1381–1403 (1325–1348).
- Elburg, M.A., Kamenetsky, V.S., Foden, J.D., Sobolev, A., 2007. The origin of medium-K ankaramitic arc magmas from Lombok (Sunda arc, Indonesia): Mineral and melt inclusion evidence. *Chem. Geol.* 240, 260–279.
- England, F., Wilkins, C., 2004. A simple analytical approximation to the temperature structure in subduction zones. *Geophys. J. Int.* 159 (3), 1138–1154.
- Fedak, S.I., Turkin, Yu.A., Gusev, A.I., Shokal'skii, S.P., Rusanov, G.G., Borisov, B.A., Belyaev, G.M., Leont'eva, E.M., 2011. An Explanatory Note. State Geological Map of the Russian Federation, Scale 1:1,000,000 (Third Generation). Altai–Sayan Series. Sheet M-45: Gorno-Altaiisk [in Russian]. Izd. VSEGEI, St. Petersburg.
- Flower, F.J., 1973. Evolution of basaltic and differentiated lavas from Anjouan, Comores Archipelago. *Contrib. Mineral. Petrol.* 38, 237–260.
- Frey, F.A., Green, D.H., Roy, S.D., 1978. Integrated models of basalt petrogenesis: a study of quartz tholeiites to olivine melilitites from south eastern Australia utilizing geochemical and experimental petrological data. *J. Petrol.* 19, 463–513.
- Gibsher, A.S., Esin, S.V., Izokh, A.E., Kireev, A.D., Petrova, T.V., 1997. Cambrian diopside-bearing basalts of the Cheposh zone in Gorny Altai: a model for fractionation of hybrid magmas in intermediate magmatic chambers. *Geologiya i Geofizika (Russian Geology and Geophysics)* 38 (11), 1760–1772 (1789–1802).
- Gioncada, A., Clocchiatti, R., Sbrana, A., Bottazzi, P., Massare, D., Ottolini, L., 1998. A study of melt inclusions at Vulcano (Aeolian islands, Italy): Insights on the primitive magmas and on the volcanic feeding system. *Bull. Volcanol.* 60, 286–306.
- Gottman, I.A., Pushkarev, E.V., Kamenetskii, V.S., Ryazantsev, A.V., 2016. Composition of magmatic inclusions in porphyritic Cr-spinel phenocrysts from the South Urals ankaramites, in: Yearbook: Transactions of the Institute of Geology and Geochemistry UB RAS [in Russian]. Issue 163, pp. 86–91.
- Green, D.H., Schmidt, M.W., Hibberson, W.O., 2004. Island-arc ankaramites: Primitive melts from fluxed refractory lherzolitic mantle. *J. Petrol.* 45, 391–403.
- Gunn, M.B., Coy-Yll, R., Watkins, N.D., Abranson, C.E., Nougier, J., 1970. Geochemistry of the oceanite–ankaramite–basalt suite from East Island, Crozet Archipelago. *Contrib. Mineral. Petrol.* 28, 319–339.
- Hammer, J., Jacob, S., Welsch, B., Hellebrand, E., Sinton, J., 2016. Clinopyroxene in postshield Haleakala ankaramite: 1. Efficacy of thermobarometry. *Contrib. Mineral. Petrol.* 171, issue1, article 7.
- Hughes, C.J., 1982. *Igneous Petrology*. Elsevier, Amsterdam.
- Irvine, T.N., 1973. Bridget Cove volcanics, Juneau area, Alaska: possible parental magma of Alaskan-type ultramafic complexes, in: Carnegie Institution of Washington. Year Book 72, pp. 478–491.
- Izokh, A.E., Borisenko, A.S., Goverdovskii, V.A., Tolstikh, N.D., Slutsker, E.M., 2004. The Ordovician Kuznetsk-Alatau–Altai platiniferous belt (Altai–Sayan folded area–western Mongolia), in: Geodynamic Evolution of the Lithosphere of the Central Asian Mobile Belt (from Ocean to Continent). Proceedings of Scientific Workshop on the Basic Research Program, Irkutsk, 19–22 October 2004 [in Russian]. Izd. IG SO RAN, Irkutsk, Vol. 1, pp. 141–142.

- Izokh, A.E., Vishnevskii, A.V., Polyakov, G.V., Kalugin, V.M., Oyunchimeg, T., Shelepaev, R.A., Egorova, V.V., 2010. The Ureg Nuur Pt-bearing volcanoplutonic picrite–basalt association in the Mongolian Altay as evidence for a Cambrian–Ordovician Large Igneous Province. *Russian Geology and Geophysics (Geologiya i Geofizika)* 51 (5), 521–533 (665–681).
- Kamenetsky, V.S., Eggins, S.M., Crawford, A.J., Green, D.H., Gasparon, M., Falloon, T.J., 1998. Calcic melt inclusions in primitive olivine at 43°N MAR: evidence for melt–rock reaction/melting involving clinopyroxene-rich lithologies during MORB generation. *Earth Planet. Sci. Lett.* 160, 115–132.
- Kamenetsky, V.S., Crawford, A.J., Meffre, S., 2001. Factors controlling the chemistry of magmatic spinel: An empirical study of associated olivine, Cr-spinel and melt inclusions from primitive rocks. *J. Petrol.* 42, 655–671.
- Kennedy, A.K., Hart, S.R., Frey, F.A., 1990. Composition and isotopic constraints on the petrogenesis of alkaline arc lavas: Lihir Island, Papua New Guinea. *J. Geophys. Res.* 95, 6929–6942.
- Kogiso, T., Hirschmann, M.M., 2001. Experimental study of clinopyroxene partial melting and the origin of ultra-calcic melt inclusions. *Contrib. Mineral. Petrol.* 142, 347–360.
- Lacroix, A., 1916. Sur quelques roches volcaniques mélanocrates des Possessions françaises de l’océan Indien et du Pacifique. *C.R. Acad. Sci. Paris* 158, 177–183.
- Lavrent’ev, Yu.G., Karmanov, N.S., Usova, L.V., 2015. Electron probe microanalysis of minerals: Microanalyzer or scanning electron microscope? *Russian Geology and Geophysics (Geologiya i Geofizika)* 56 (8), 1154–1161 (1473–1482).
- Laz’ko, E.E., Sharkov, E.V., 1988. *Igneous Rocks. Ultrabasic Rocks* [in Russian]. Nauka, Moscow, Vol. 5.
- Le Maitre, R.W., Streckeisen, A., Zanettin, B., Le Bas, M.J., Bonin, B., Bateman, P., Bellieni, G., Dudek, A., Efremova, S., Keller, J., Lame-re, J., Sabine, P.A., Schmid, R., Sorensen, H., Woolley, A.R., 2002. *Igneous rocks: a classification and glossary of terms. Recommendations of the International Union of Geological Sciences, Subcommittee on the Systematics of Igneous Rocks.* Cambridge University Press, Cambridge.
- Maaløe, S., Sorensen, I., Hartogen, J., 1986. The trachybasaltic suite of Jan Mayen. *J. Petrol.* 27, 439–466.
- Marchev, P., Georgiev, S., Zajac, Z., Manetti, P., Raicheva, R., Von Quadt, A., Tommasini, S., 2009. High-K ankaramitic melt inclusions and lavas in the Upper Cretaceous Eastern Srednogorie continental arc, Bulgaria: Implication for the genesis of arc shoshonites. *Lithos* 113, 228–245.
- Médard, E., Schmidt, M.W., Schiano, P., 2004. Liquidus surfaces of ultracalcic primitive melts: formation conditions and sources. *Contrib. Mineral. Petrol.* 148, 201–215.
- Médard, E., Schmidt, M.W., Schiano, P., Ottolini, L., 2006. Melting of amphibole-bearing wehrlites: An experimental study on the origin of ultra-calcic nepheline-normative melts. *J. Petrol.* 47, 481–504.
- Morimoto, N., 1988. Nomenclature of pyroxenes. *Am. Mineral.* 73, 1123–1133.
- Mossman, D.J., Coombs, D.S., Kawachi, Y., Reay, A., 2000. High-Mg arc-ankaramitic dikes, Greenhills Complex, Southland, New Zealand. *Can. Mineral.* 38, 191–216.
- Ortiz Hernández, L.E., 2000. An arc ankaramite occurrence in central Mexico. *Revista Mexicana de Ciencias Geológicas* 17 (1), 34–44.
- Oyunchimeg, T., Izokh, A.E., Vishnevsky, A.V., Kalugin, V.M., 2009. Isoferroplatinum mineral assemblage from the Burgastain Gol placer (Western Mongolia). *Russian Geology and Geophysics (Geologiya i Geofizika)* 50 (10), 863–872 (1119–1130).
- Portnyagin, M.V., Plechov, P.Y., Matveev, S.V., Osipenko, A.B., Mironov, N.L., 2005a. Petrology of avachites, high-magnesian basalts of Avachinsky volcano, Kamchatka: I. General characteristics and composition of rocks and minerals. *Petrology* 13 (2), 99–121.
- Portnyagin, M.V., Mironov, N.L., Matveev, S.V., Plechov, P.Y., 2005b. Petrology of avachites, high-magnesian basalts of Avachinsky Volcano, Kamchatka: II. Melt inclusions in olivine. *Petrology* 13 (4), 322–351.
- Pushkarev, E.V., Gottman, I.A., 2016. Composition of porphyritic Cr-spinel phenocrysts in clinopyroxene porphyrites of the Irendyk Formation (South Urals) as an indicator of the ankaramitic nature of volcanic rocks. *Vestnik UrO RAN Rossiiskogo Mineralogicheskogo Obshchestva*, No. 13, 112–120.
- Pushkarev, E.V., Ryazantsev, A.V., Gottman, I.A., 2017. Ankaramites of the Sakmara–Voznesenka zone (South Urals): geologic location and composition, in: *Yearbook: Transactions of the Institute of Geology and Geochemistry UB RAS* [in Russian]. Issue 164, pp. 166–175.
- Pushkarev, E.V., Ryazantsev, A.V., Gottman, I.A., Degtyarev, K.E., Kamenetskiy, V.S., 2018. Ankaramite: a new type of high-magnesium and high-calcium primitive melt in the Magnitogorsk island-arc zone (Southern Urals). *Dokl. Earth Sci.* 479 (2), 463–467.
- Ringwood, A.E., 1975. *Composition and Petrology of the Earth’s Mantle.* McGraw-Hill, London, New York, Sydney.
- Safonova, I.Yu., Buslov, M.M., Simonov, V.A., Izokh, A.E., Komiya, Ts., Kurganskaya, E.V., Ohno, T., 2011. Geochemistry, petrogenesis, and geodynamic origin of basalts from the Katun’ accretionary complex of Gorny Altai (southwestern Siberia). *Russian Geology and Geophysics (Geologiya i Geofizika)* 52 (4), 421–442 (541–567).
- Schiano, P., Eiler, J.M., Hutcheon, I.D., Stolper, E.M., 2000. Primitive CaO-rich, silica-undersaturated melts in island arcs: Evidence for the involvement of clinopyroxene-rich lithologies in the petrogenesis of arc magmas. *Geochem. Geophys. Geosyst.* 1, 1999GC000032.
- Schmidt, M.W., Green, D.H., Hibberson, W.O., 2004. Ultra-calcic magmas generated from Ca-depleted mantle: an experimental study on the origin of ankaramites. *J. Petrol.* 45, 531–554.
- Simonov, V.A., Safonova, I.Yu., Kovyazin, S.V., Kurganskaya, E.V., 2010. Physicochemical parameters of petrogenesis of basalt complexes in the Katun’ zone, Gorny Altai. *Litosfera*, No. 3, 111–117.
- Sisson, T.W., Bronto, S., 1998. Evidence for pressure release melting beneath magmatic arcs from basalts at Galunggung, Indonesia. *Nature* 391, 883–886.
- Sorbadere, F., Schiano, P., Métrich, N., 2013. Constraints on the origin of nepheline-normative primitive magmas in island arcs inferred from olivine-hosted melt inclusion compositions. *J. Petrol.* 54, 215–233.
- Thompson, N., Flower, F.J., 1971. Evidence for upper-crust ankaramitic liquids. *Am. Geophys. Union Trans.* 52, 377.
- Tolstykh, N.D., 2004. *Mineral Assemblages of Platinum Placers and Genetic Correlations with Their Source Rocks.* ScD Thesis [in Russian]. Novosibirsk.
- Vrublevskii, V.V., Krupchatnikov, V.I., Izokh, A.E., Gertner, I.F., 2012. The alkaline and carbonatitic rocks of Gorny Altai (Edel’veis complex) as indicators of Early Paleozoic plume magmatism in the Central Asian Fold Belt. *Russian Geology and Geophysics (Geologiya i Geofizika)* 53 (8), 721–735 (945–963).
- White, R.S., McKenzie, D., O’Nions, R.K., 1992. Oceanic crustal thickness from seismic measurements and rare earth element inversions. *J. Geophys. Res.* 97, 19683–19715.
- Zhang, Z., Mao, J., Cai, J., Kusky, T.M., Zhou, G., Yan, S., Zhao, L., 2008. Geochemistry of picrites and associated lavas of a Devonian island arc in the northern Junggar terrane, Xinjiang (NW China): Implications for petrogenesis, arc mantle sources and tectonic setting. *Lithos* 105, 379–395.
- Zhmodik, S.M., Nesterenko, G.V., Airiyants, E.V., Belyanin, D.K., Kolpakov, V.V., Podlipsky, M.Yu., Karmanov, N.S., 2016. Alluvial platinum-group minerals as indicators of primary PGE mineralization (placers of southern Siberia). *Russian Geology and Geophysics (Geologiya i Geofizika)* 57 (10), 1437–1464 (1828–1860).
- Zybin, V.A., 2006. *The Reference Ust’-Sema Complex of Natural Basalts and Trachybasalts (Gorny Altai)* [in Russian]. SNIIGiMS, Novosibirsk.